The role of variable slab dip in driving mantle flow at the eastern edge of the Alaskan subduction margin: insights from SKS shear-wave splitting

C.M.A. Venereau [1,2], R. Martin-Short [2], I.D. Bastow [1], R.M. Allen [2], R. Kounoudis [1]

[1]Imperial College London, Department of Earth Science and Engineering

[2]University of California Berkeley Seismological Laboratory

Key Points:

- Fast directions parallel major transform faults and Yakutat terrane subduction, suggesting a lithospheric source of anisotropy.
- Fast directions wrapping around the slab edge and high delay times suggest a toroidal asthenospheric flow as another cause of anisotropy.
- Variability in slab geometry exerts first order control over mantle flow at the edge of the Alaskan margin.

Corresponding author: R. Martin-Short, martinshortr@gmail.com

This article has been accepted for publication and undergone full peer review but has not been through the copyediting, typesetting, pagination and proofreading process which may lead to differences between this version and the Version of Record. Please cite this article as doi: 10.1029/2018GC008170

©2018 American Geophysical Union. All rights reserved.

Accepted Article

Abstract

Alaska provides an ideal tectonic setting for investigating the interaction between subduction and asthenospheric flow. Within the span of a few hundred kilometers along-strike, the geometry of the subducting Pacific plate varies significantly and terminates in a sharp edge. Furthermore, the region documents a transition from subduction along the Aleutian Arc to strike-slip faulting along the Pacific Northwest. To better understand mantle interactions within this subduction zone, we conduct an SKS shear-wave splitting analysis on passive-source seismic data collected between 2011 and 2018 at 239 broadband seismometers, including those from the Transportable Array (TA). Anisotropic fast directions in the east of our study area parallel the Queen Charlotte and Fairweather transform faults, suggesting that the ongoing development of lithospheric anisotropy dominates the results there. However, our observed delay times ($\delta t = 1$–1.5 s) obtained across the study region may also imply an asthenospheric contribution to the splitting pattern. Our splitting observations exhibit slab-parallel fast directions north-west of the trench and a rotation of fast directions around the north-eastern slab edge. These observations suggest the presence of toroidal asthenospheric flow around the edge of the down-going Pacific plate. We suggest that Wrangell Volcanic Field (WVF) volcanism might be caused by mantle upwelling associated with this flow. Splitting observations closer to the trench can be explained by fossil anisotropy within the downgoing Pacific-Yakutat plate combined with entrained sub-slab mantle. The geometry of the slab, including its variable dip and its abrupt eastern edge, thus plays an important role in governing mantle flow beneath Alaska.

1 Introduction

The tectonics of southern Alaska are dominated by the northward subduction of the Pacific plate beneath the North American plate (Figure 1). South-central Alaska exhibits a so-called "corner geometry" because it lies at the north-eastern vertex of the Pacific plate, which is bounded to the east by transform faults and to the north by subduction [*Eberhart-Phillips et al.*, 2006; *Jadamec and Billen*, 2010]. Here, the Pacific plate subducts beneath North America at a rate of ~50 mm/yr [*Sauber*, 1997]. Active volcanism is abundant in Alaska but its relationship to subduction is debated [e.g., *Martin-Short et al.*, 2016]. The subduction geometry is heterogeneous along strike, transitioning from a steeply dipping slab under the Aleutians to shallow subduction at the eastern end of the subduction zone, which is associated with a paucity of volcanism known as the De-

Accepted Article

©2018 American Geophysical Union. All rights reserved.

Accepted Article

nali Gap [*Nye*, 1999; *Christenson et al.*, 2010; *Rondenay et al.*, 2010; *Martin-Short et al.*, 2016]. This setting is further complicated by active collision and accretion of the Yakutat terrane (Figure 1), which is occurring at the easternmost boundary of the subduction zone [*Eberhart-Phillips et al.*, 2006; *Wang and Tape*, 2014]. The Yakutat terrane is a region of over-thickened oceanic crust that has been converging with the Alaskan margin for ≥ 23 Ma, and has led to broad continental deformation and uplift of the coastal Chugach-St. Elias ranges ~~range~~ [*Christenson et al.*, 2010; *Plafker and Berg*, 1994; *Koons et al.*, 2010]. Furthermore, subduction of the thick, buoyant, Yakutat crust is believed to have caused the flattening of the subducting slab and cessesion of volcanism in the Denali Gap [*Christenson et al.*, 2010; *Plafker and Berg*, 1994]. The variation of mantle flow geometry along strike beneath the Alaskan margin is poorly constrained. South-central Alaska is therefore an ideal place to study the interaction between present-day mantle flow and varying subduction geometries.

A further unexplained tectonic feature of the region is the Wrangell Volcanic Field (WVF: Figure 1), which lies just east of the eastern edge of the subducted Yakutat terrane. The WVF has experienced a northwestward progression of volcanic activity over its history [*Richter et al.*, 1990], perhaps associated with the subduction of Yakutat crust beneath Alaska. Many of the lavas sampled from the WVF exhibit a transitional or calc-akaline affinity suggestive of arc magmatism, with the anomalous presence of adakitic and tholeiitic lavas in some locations [*Preece and Hart*, 2004]. There is little seismic evidence for subducted material beneath the WVF and its causes remain unknown [*Martin-Short et al.*, 2016]. 3D geodynamic modeling by *Jadamec and Billen* [2010, 2012] predicts vertical upwelling beneath the WVF associated with quasi-toroidal mantle flow around the slab edge, potentially explaining the volcanism in the area. Furthermore, the tomographic imaging of *Martin-Short et al.* [2018] suggests that the WVF lies directly above the eastern edge of the subducted Yakutat terrane, potentially explaining its unusual characteristics. The geochemical study of *Brueseke et al.* [2019] also shows that subducting slab-edge upwelling and flat-slab defocused fluid-flux are mechanisms which might explain volcanism at the WVF.

Studies of seismic anisotropy in this region will provide insights into mantle deformation geometry, the origins of volcanism, and will help test predictions from previous geodynamic modeling of 3D asthenospheric flow in the area [e.g. *Jadamec and Billen*, 2010, 2012]. When a shear-wave enters an anisotropic medium, it splits into two orthog-

©2018 American Geophysical Union. All rights reserved.

onally polarized components that travel at different speeds and accumulate a delay time [e.g., *Silver and Chan*, 1991]. The delay time δt between the fast and slow components reflects the strength of anisotropy and the thickness of the anisotropic medium [e.g., *Silver and Chan*, 1991]. The teleseismic phases SKS, SKKS and PKS are ideal for investigating upper mantle anisotropy because these phases exhibit near-vertical ray paths on the receiver side of the Earth, thus sampling anisotropy directly beneath the stations. Such measurements represent the path-integrated effect of anisotropy from the core-mantle boundary (CMB) to the surface [e.g., *Silver and Chan*, 1991]. Due to mode conversion at the CMB, the SKS, SKKS and PKS phase analysis yields measurements that are not contaminated by source-side anisotropy. In the upper mantle, seismic anisotropy occurs due to the development of lattice-preferred orientation (LPO) of anisotropic minerals such as olivine [e.g., *Karato et al.*, 2008]. In the absence of shearing, the crystallographic fast axes of these mineral grains are randomly oriented. However, in the asthenosphere, simple shear imposed by plate motions or other macroscopic influences can encourage large-scale alignment of the crystallographic fast axes. For example, under typical asthenospheric conditions below stable lithosphere and in the presence of simple shear caused by plate motion, the fast axes direction of shear-wave splitting (ϕ) is generally aligned with the direction of maximum shearing, which can be indicative of flow in the asthenosphere [*Silver and Chan*, 1991; *Hall et al.*, 2000]. However, in atypical mantle conditions, such as the relatively low temperature, high water-content environment that exists within parts of the mantle wedge at subduction zones, the fast direction may instead align perpendicular to the direction of maximum shear stress [*Karato et al.*, 2008]. This is known as B-type fabric. Furthermore, shear-wave splitting may also result from fossil anisotropy in the lithosphere [e.g., *Silver and Chan*, 1988; *Darbyshire et al.*, 2015; *Gilligan et al.*, 2016] or aligned structural heterogeneities (shape preferred orientation) such as melt intrusions [e.g., *Blackman and Kendall*, 1997; *Bastow et al.*, 2010; *Holtzman et al.*, 2010]. Hence, care must be taken in discerning the main source of the anisotropic signal.

We present a teleseismic shear-wave splitting study of lithospheric and asthenospheric anisotropy in south-central Alaska using data from 239 broadband seismometers, including the newly-installed Transportable Array instruments (see acknowledgments for detailed references). The station coverage is such that we are able to investigate a region of steeply dipping slab, a region of flat-slab subduction, the abrupt slab edge and the transition from subduction to transform faulting along the Pacific Northwest. Our shear-wave

©2018 American Geophysical Union. All rights reserved.

Accepted Article

splitting study is the first of its type to have such extensive spatial coverage across south-central Alaska. By presenting additional splitting measurements spanning most of mainland Alaska, our study expands on and is in agreement with previous shear-wave splitting studies in this region [e.g. *Christensen and Abers*, 2009; *Hanna and Long*, 2012; *Perttu et al.*, 2014], therefore providing important new constraints on present-day mantle flow in the region.

2 Tectonic Framework

The Alaskan lithsophere comprises several geologic terranes of various compositions, which have been sutured to the northwestern margin of Laurentia since the late Triassic [e.g. *Plafker and Berg*, 1994] (Figure 1). The geology documents a complex tectonic history of volcanic arc accretion, subduction zone migration and movement along major strike-slip faults [*Colpron*, 2007; *O'Driscoll and Miller*, 2015; *Moore and Box*, 2016].

The oldest rocks in Alaska are Proterozoic-to-Triassic miogeoclinal sediments deposited at the edge of the Laurentian margin [*Colpron*, 2007]. Over the past 200 Ma, the region has grown mainly though accretion of volcanic, metamorphic and plutonic assemblages which have been brought to their modern positions though a combination of subduction and migration along right-lateral strike slip faults [*Plafker and Berg*, 1994; *Nokleberg et al.*, 2000]. The accretion of terranes began with the Yukon Composite Terrane (YCT) in the Triassic, followed by the Arctic-Alaska Terrane (AAT) and Ocean Domain Terrane (ODT), which make up the northern and north-western segments of Alaska [*Colpron*, 2007; *Nokleberg et al.*, 2000] (Figure 1). The southern margin of Alaska has been a site of northwards-verging subduction since the early Jurassic [*Plafker and Berg*, 1994]. [*Finzel et al.*, 2011] describe its southwards growth in the context of three major accretion events: The Wrangellia composite Terrane (WCT; mid–late Jurrassic), the Chugach Terrane (Cretaceous) and the Yakutat Terrane (collision ongoing) [*Moore and Box*, 2016].

The Yakutat terrane is a region of thick (>20 km) oceanic crust, thought to have formed as an oceanic plateau 1500-2000 km to the south of its current position [e.g. *Plafker and Berg*, 1994]. It was subsequently rafted north by motion on the Queen Charlotte/Fairweather transform system [*Worthington et al.*, 2012] and has been subducting beneath the southern margin of Alaska for at least 23 Ma [*Ferris et al.*, 2003]. Tomographic models [*Eberhart-Phillips et al.*, 2006; *Rondenay et al.*, 2010] and receiver function studies [*Ferris et al.*,

©2018 American Geophysical Union. All rights reserved.

Accepted Article

2003] reveal that thick crust of the Yakutat terrane has penetrated more than 600 km inland of the trench. Subduction of this thick, buoyant crust is likely responsible for flattening of the slab in this region, which in turn has caused broad intraplate deformation and a region of volcanic quiescence known as the Denali Volcanic Gap (DVG) [*Eberhart-Phillips et al.*, 2006; *Rondenay et al.*, 2010; *Koons et al.*, 2010; *Jadamec et al.*, 2013; *Finzel et al.*, 2015]. South of the DVG, the Aleutian-Alaska volcanic arc follows the 100 km depth contour of the subducting Pacific plate, implying a hydrated mantle wedge and sufficient pathways for melt to reach the surface [*Martin-Short et al.*, 2016]. Volcanism along this arc began ca. 55 Ma, concurrent with a southwards jump in the position of the subduction zone [*Plafker and Berg*, 1994].

Teleseismic body wave [*Martin-Short et al.*, 2016] and surface wave [*Wang and Tape*, 2014; *Martin-Short et al.*, 2018] tomography studies image the subducting lithosphere as an elongate, high-velocity anomaly that extends from the Aleutian arc into Central Alaska. These studies suggest that the eastern extent of the subducted Yakutat terrane lies at or near the edge of the down-going Pacific lithosphere, which terminates abruptly beneath South-Central Alaska [*Martin-Short et al.*, 2016, 2018]. The slab dip is relatively shallow where Yakutat crust is present, but steepens sharply beyond its northern edge [*Qi et al.*, 2007; *Martin-Short et al.*, 2016]. Numerical modeling studies such as *Jadamec and Billen* [2010] have addressed questions concerning the influence of the slab edge on asthenospheric flow geometry, and modeled a toroidal mantle flow around the slab edge. The results of our study provide further constraints by investigating the pattern of seismic anisotropy across the slab edge, allowing comparison over a large area of the model domain of *Jadamec and Billen* [2010].

©2018 American Geophysical Union. All rights reserved.

Accepted Article

Accepted Article

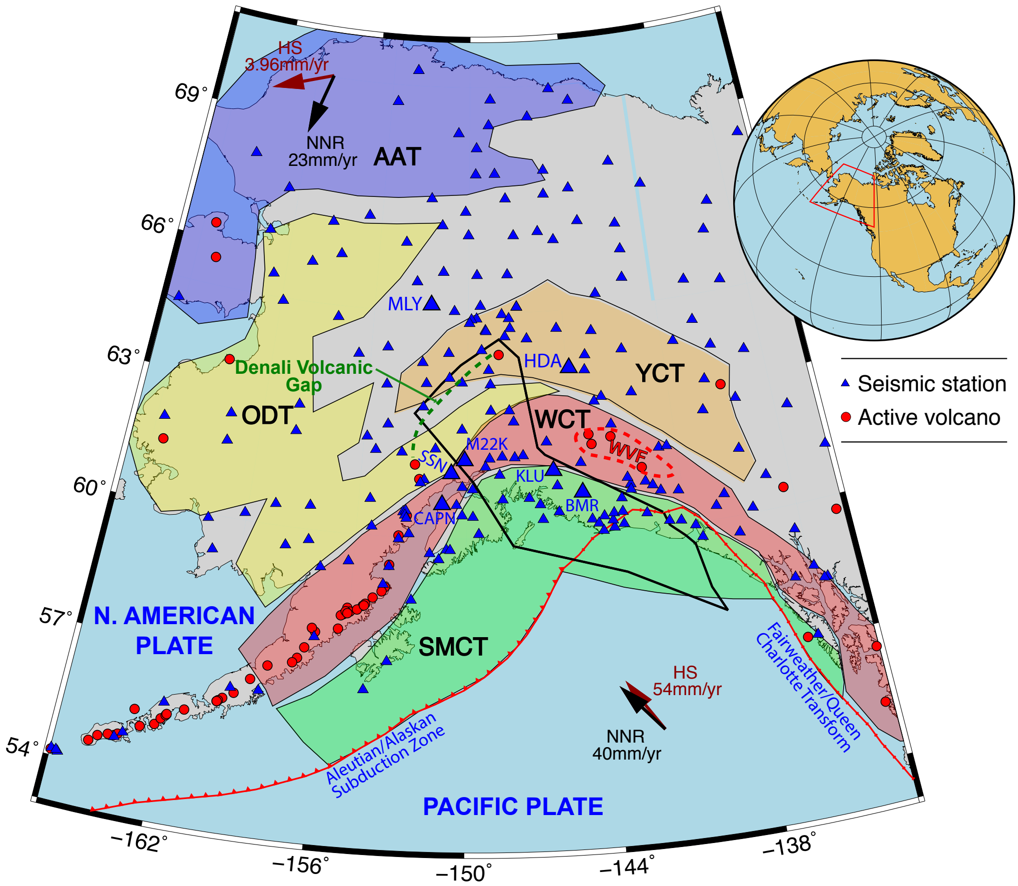

Figure 1. Seismic stations used in this study (blue triangles) and composite geological terranes of Alaska. The extent of the subducted Yakutat terrane as estimated by *Eberhart-Phillips et al.* [2006] is outlined in black; its northwestern-most boundary delineates the Denali Gap, where there is an absence of volcanism, despite the ample evidence for subduction. Stations AK stations CAPN, SSN, HDA, KLU, BMR and MLY are labeled, in addition to TA station M22K. Solid arrows show the direction of absolute plate motion (APM) in the hot spot (HS) and no-net rotation (NNR) reference frames [*Gripp and Gordon*, 2002]. Colored polygons show the approximate extents of the five major composite terranes discussed in this paper: SMCT; Southern Margin Composite Terrane, WCF; Wrangellia Composite Terrane, YCT; Yukon Composite Terrane, ODT; Ocean Domain Terrane, AAT; Arctic Alaska Terrane [*Colpron et al. 2007; Martin-Short et al. 2018*]. Green dashed line: the Denali Volcanic Gap; Red dashed line: the Wrangell Volcanic Field (WVF).

©2018 American Geophysical Union. All rights reserved.

Accepted Article

3 Data Selection and Shear-Wave Splitting Analysis

Our teleseismic dataset was obtained from the IRIS Data Management Center (DMC) and comprised all broadband seismograph stations in the region spanning 166-133°W and 53–72°N. This included the AK, AT, AV, CN, IM, NY, TA, XV, YE, and ZE networks. We inspected seismograms of SKS and SKKS phases for earthquakes of mb≥6 occurring at epicentral distances of ≥88° from 2011 to 2018 (Figure 2). We also inspected all earthquakes of mb≥5.7–5.9 of depth >400km. In total 2233 earthquake-station pairs were examined, and 582 were incorporated in the final dataset (Figure 2). Seismograms were filtered prior to splitting analysis using a zero-phase Butterworth bandpass filter with corner frequencies of 0.04 and 0.3 Hz. Splitting parameters were constrained using the semi-automated method of *Teanby et al.* [2004], which is based on the *Silver and Chan* [1991] approach. The horizontal components are rotated and time-shifted to minimize the second eigenvalue of the covariance matrix for particle motion within a time window around the SKS pulse. This is equivalent to linearizing the particle motion and minimizing the tangential component of the shear wave energy. A so-called ‘null’ measurement results when the particle motion is linearized initially. Nulls indicate that the anisotropic fast direction is either perpendicular or parallel to the backazimuth of the wave, or that the mantle below the station is isotropic. Null measurements therefore have an inherent 90° ambiguity. The *Silver and Chan* [1991] approach takes a single, manually picked, shear-wave analysis window. In the cluster analysis approach of *Teanby et al.* [2004], however, the splitting analysis is performed for a range of window lengths and cluster analysis is utilized to find measurements that are stable over many different windows. All splitting parameters were determined after analysis of 100 different windows. Once clusters of stable results have been found, the final choice of ϕ and δt corresponds to the measurement with the lowest error (determined via an F-test to calculate the 95% confidence interval for the optimum values for ϕ and δt) in the cluster with the smallest variance. Figure 3 shows an example of the analysis, while Figure 4 shows an example of a null.

We typically obtained between 2 and 6 good quality splitting measurements per station. The backazimuthal distribution of station-earthquake pairs is uneven, with earthquake locations dominantly in the western Pacific (Figure 2). This limits our ability to resolve complex patterns of seismic anisotropy such as dipping or multiple anisotropic layers, which manifest as backazimuthal variations in ϕ and δt [e.g., *Savage and Silver*, 1993; *Liddell et al.,* 2017].

©2018 American Geophysical Union. All rights reserved.

Accepted Article

For stations where we have good backazimuthal coverage, we find relatively little evidence for variations in ϕ and δt, though some stations (e.g., E24K, MLY) do show some evidence of variation (Figure 5; see supporting information for a full set of these plots). Abrupt changes in ϕ and δt over very short ($< 20°$) backazimuth ranges would be diagnostic of a two-layer, rather than a dipping layer anisotropic model (e.g., Liddell et al., 2017), but the lack of evidence for such patterns means discriminating between layered and dipping fabric anisotropic models would be speculative a best.

To obtain a single pair of splitting parameters per station (which we acknowledge assumes a single, horizontal, homogeneous anisotropic layer hypothesis), we use of the error matrix stacking procedure of *Wolfe and Silver (1998).* In the stack, increased weighting is assigned to higher signal-to-noise ratio results, allowing them to exert greater control on the determined splitting parameters.

Several seismograph stations used in this study have associated instrument misorientations [*Hanna and Long*, 2012]. As far as we have been able to determine, these usually time-dependent component azimuth issues are accurately reported by the IRIS DMC in the seismogram headers, which our splitting analysis takes account of. In any case, we omit any splitting measurements from our analysis whose incoming SKS polarization azimuth does not closely parallel ($\leq 15°$) the great circle path defined by the earthquake backazimuth.

4 Shear-Wave Splitting Results

Supporting information table T1 contains the splitting measurements determined at all stations, in addition to stacks for each station and their associated uncertainties.

Our splitting results are shown in Figure 6, superimposed on a 200 km depth slice through the S-wave mantle tomographic model of *Martin-Short et al.* [2016]. This depth slice was chosen because it clearly shows the location of the subducted slab within the asthenosphere, which is interpreted to be the most significant source of the observed anisotropic signal (sections 5.4 and 5.5). The subducting Pacific plate appears as an elongate, high-velocity (blue) anomaly that extends beneath the Aleutian volcanic arc and into south-central Alaska. As demonstrated by *Martin-Short et al.* [2016], the tomographic model has sufficient resolution to resolve features of the scale of the subducting Pacific plate. Our splitting delay times range from $\delta t = 0.4$–1.95 s.

©2018 American Geophysical Union. All rights reserved.

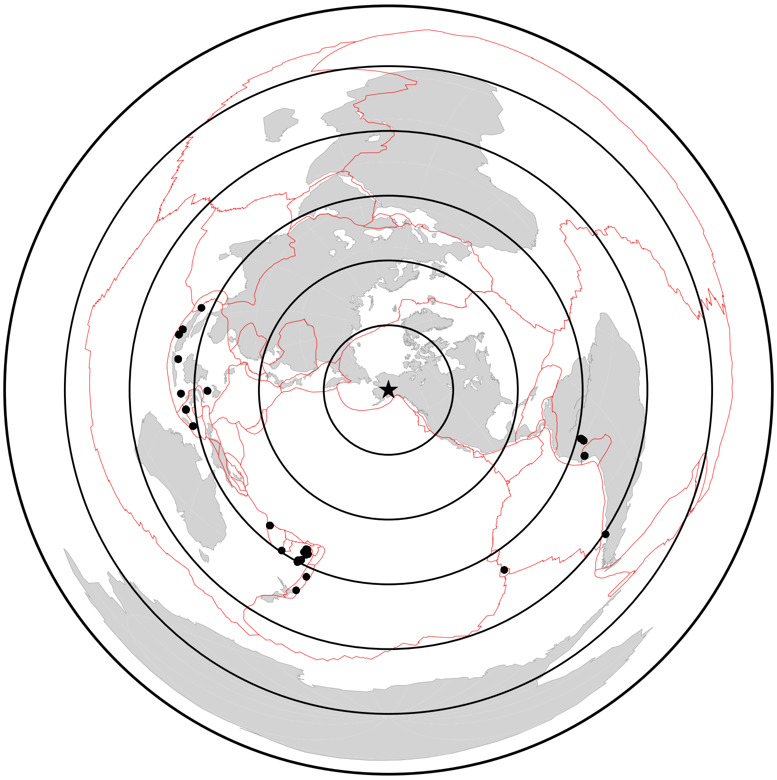

Figure 2. The global distribution of all the earthquakes (black dots) used in the study plotted with an azimuthal equidistant map projection. Red lines are plate boundaries from the model of *Bird* [2003]. The star marks the center of the seismometer network we used.

Our results can be grouped in three broad categories. Firstly, we observe a pattern of fast directions generally parallel to the strike of the subducting slab, which we refer to thereafter as slab-parallel, north-west of the slab. Secondly, at the north-eastern edge of the slab, these slab-parallel fast directions fan out and rotate around to the south, producing an arcuate pattern of rotating fast directions around the subducting Pacific-Yakutat plate at latitudes ~65°N, -147°W. Thirdly, closer to the trench, at stations such as CAPN, SSN or M22K (Figure 1), fast directions are predominantly slab-perpendicular, paralleling the subduction direction of the Pacific-Yakutat plate.

Accepted Article

©2018 American Geophysical Union. All rights reserved.

Accepted Article

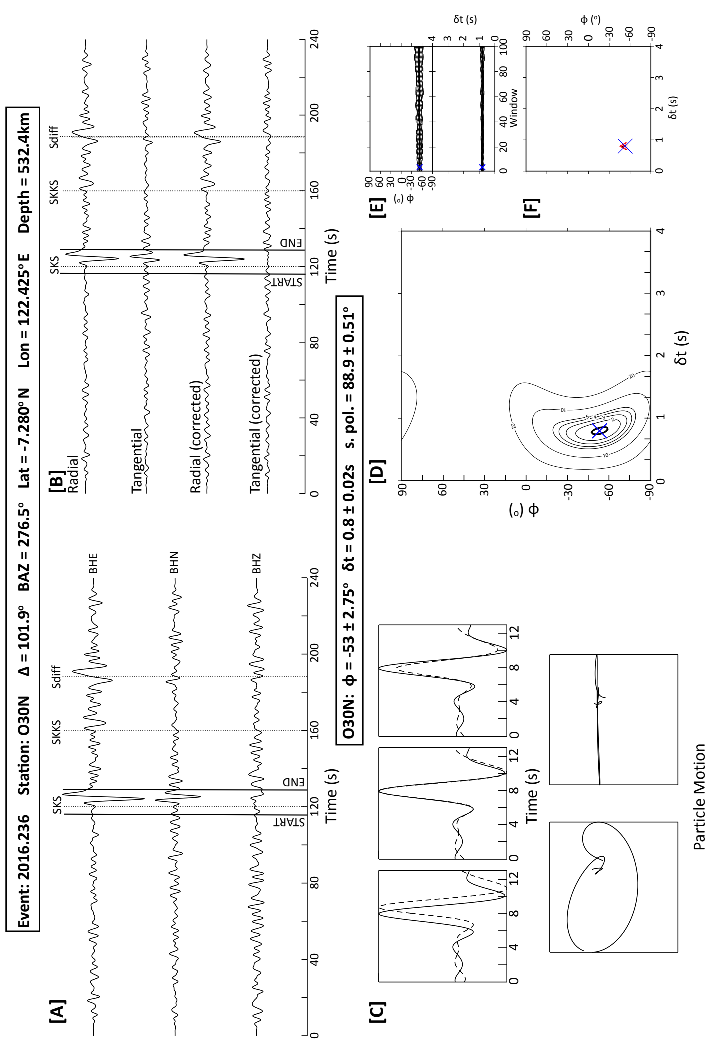

Figure 3. High-quality splitting measurement example from station O30N. (a) The recorded seismogram showing the SKS phase and the initial window. (b) The seismogram rotated into radial and tangential components both before (top two) and after (bottom two) correction with calculated splitting parameters. (c) Top L-R: close up of the SKS phases for the fast and slow waveforms before correction, after correction, and after correction without normalized amplitudes. Bottom L-R: particle motion before and after correction. (d) Contour map showing stability of the splitting parameters. Lines indicate one standard deviation. The thick line indicates the 95% confidence level. (e) Splitting parameter variations as a function of the changing window. (f) Cluster analysis results for ϕ and δt for each of the 100 windows. These values were very stable over the full range of windows.

©2018 American Geophysical Union. All rights reserved.

Accepted Article

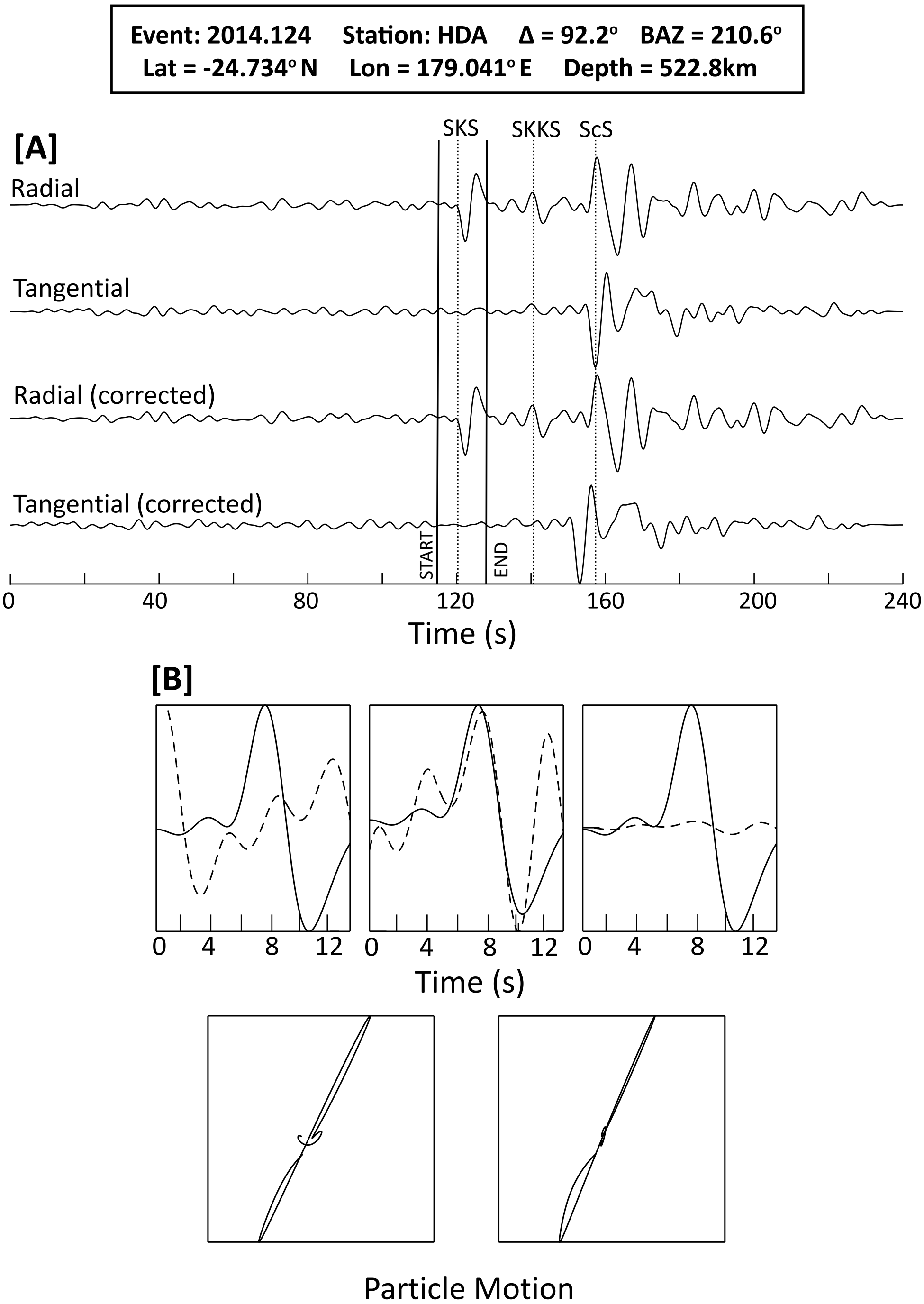

Figure 4. Example null measurement for AK station HDA. Panel A: radial and tangential components before and after the splitting analysis was performed. Panel B: Top L-R: close up of the SKS phases for the fast and slow waveforms before correction, after correction, and after correction without normalized amplitudes. Bottom L-R: particle motion before and after correction. Note the lack of tangential component energy before and after analysis, and the linear particle motion before and after analysis.

©2018 American Geophysical Union. All rights reserved.

Accepted Article

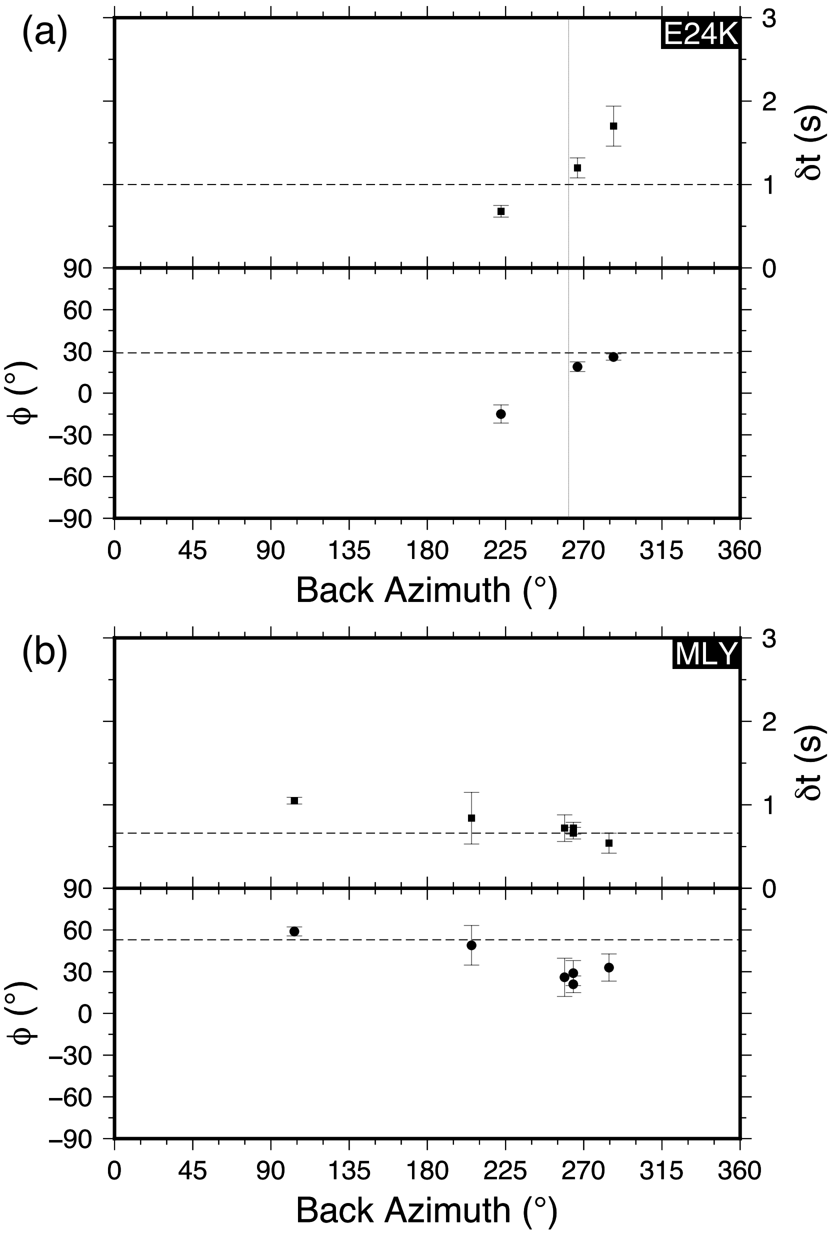

Figure 5. The distribution of splitting parameters as a function of backazimuth for (a) TA network station E24K, and (b) AK network station MLY. The dashed lines indicate the values of ϕ and δt obtained by stacking these results. Error bars show the 95% confidence interval on each measurement. See the supporting information for a full set of such plots. At many stations we only obtain splitting results from earthquakes with backazimuths close to 270°, but for those stations with a wider range of results the splitting parameters are generally consistent with backazimuth; Station E24K is one of only a few exceptions to this rule. See supporting figures S1-S218 for equivalent plots for each station in our study.

©2018 American Geophysical Union. All rights reserved.

Accepted Article

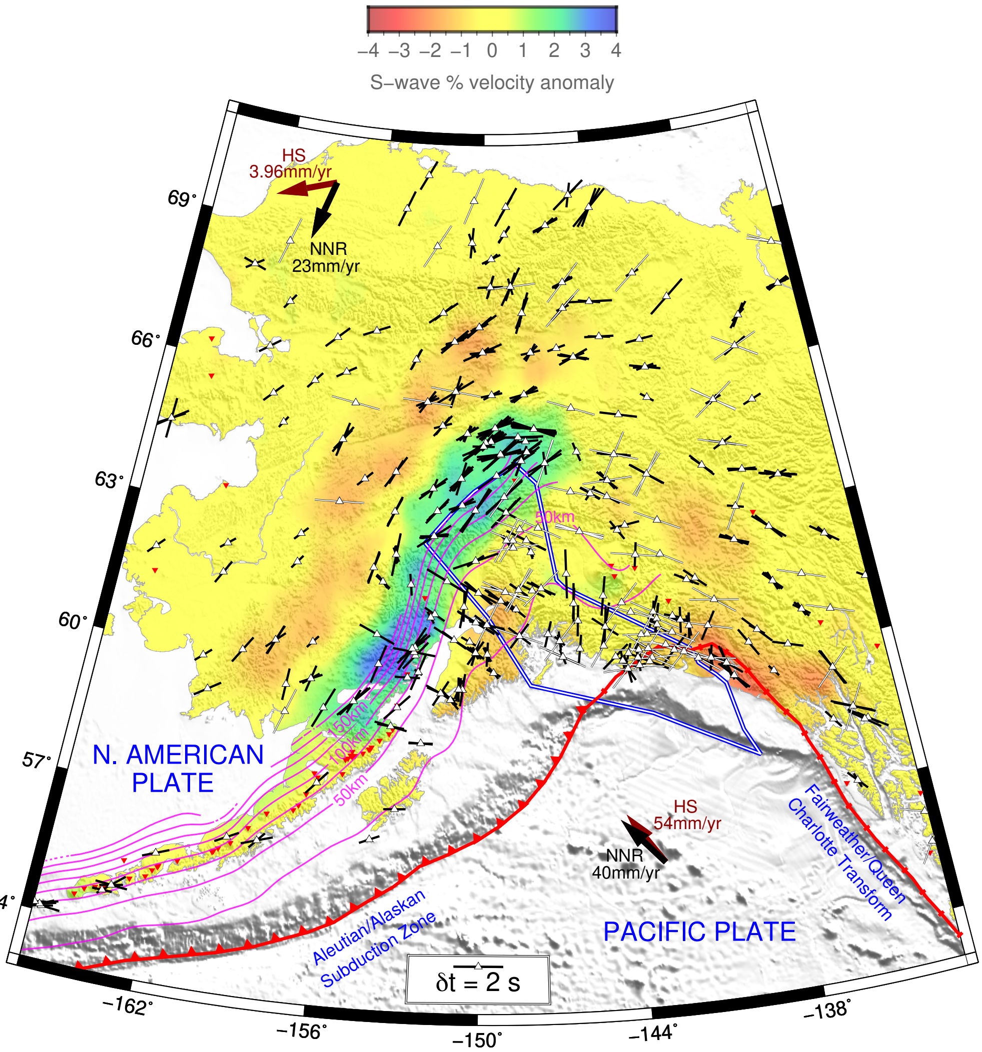

Figure 6. Shear-wave splitting observations overlain on a S-wave velocity tomographic model [*Martin-Short et al.*, 2016] depth-slice at 200 km depth. White bars are null measurements. The splitting measurements rotate around the north-east edge of the slab, identified by the elongate high velocity (blue) anomaly. The thick blue line shows the extent of the Yakutat terrane [*Eberhart-Phillips et al.*, 2006]. Solid arrows show the direction of absolute plate motion (APM) in both hot spot and no-net rotation reference frames [*Gripp and Gordon*, 2002]. Subducting slab depth contours magenta from the Slab2.0 model of *Hayes et al.* [2018] are shown in magenta. The solid thick red line marks the north American-Pacific Plate boundary. NNR and HS refer to the no-net rotation and hotspot reference frames.

©2018 American Geophysical Union. All rights reserved.

Accepted Article

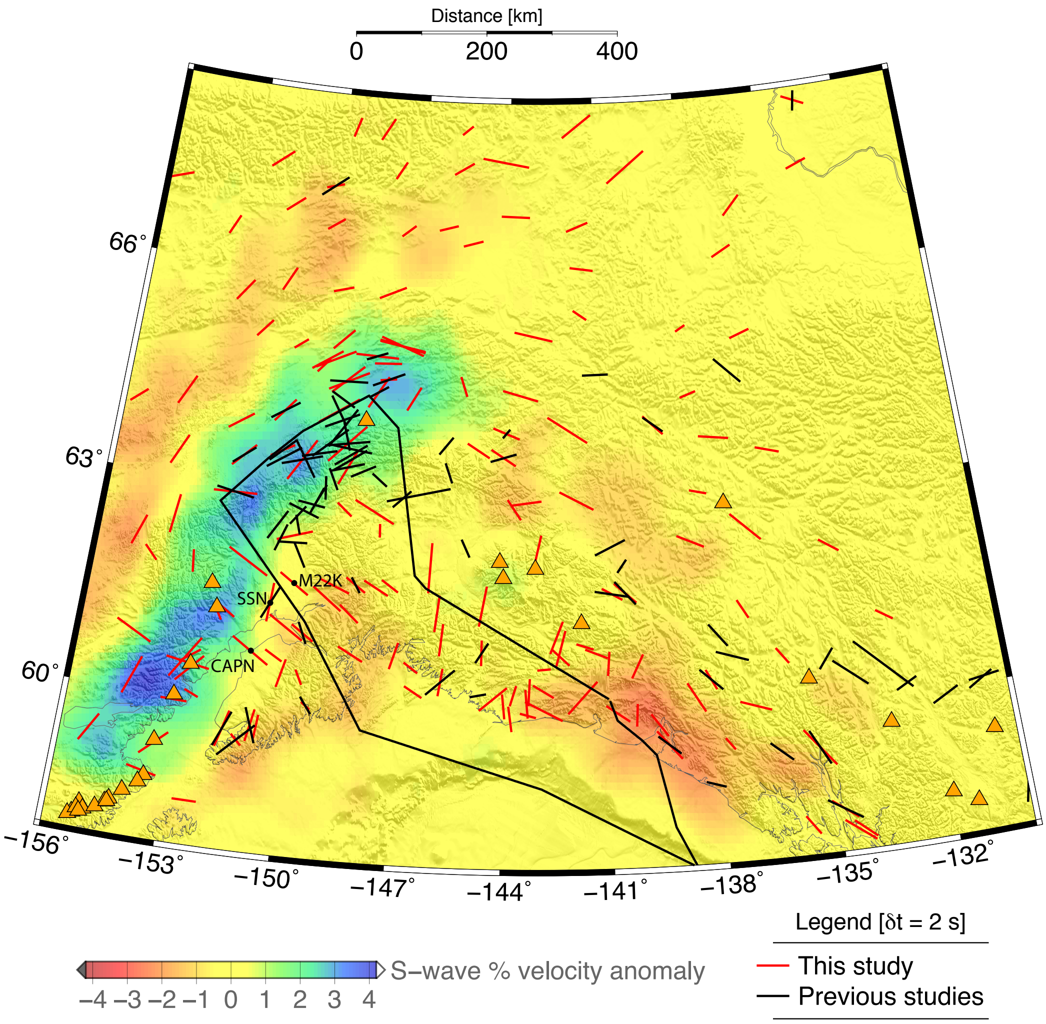

Figure 7. Comparison between the stacked splitting results obtained in our study (red) and for previous studies (black) [*Christensen and Abers*, 2009; *Hanna and Long*, 2012; *Perttu et al.*, 2014] overlain on the S-wave tomographic model of *Martin-Short et al.* [2016]. Using data from the AK array allows direct comparison between our results at these stations and results from previous studies. Orange triangles indicate active volcanoes. The extent of the Yakutat terrane [*Eberhart-Phillips et al.*, 2006] is outlined in black.

©2018 American Geophysical Union. All rights reserved.

Accepted Article

5 Discussion

5.1 Mechanisms of Seismic Anisotropy

The primary cause of seismic anisotropy in the upper mantle worldwide is the lattice preferred orientation (LPO) of olivine [e.g., *Zhang and Karato*, 1995]. LPO fabrics can develop in the asthenosphere in response to simple shear imposed by mantle flow and/or the motion of the overlying plate [e.g., *Bokelmann and Silver*, 2002; *Karato et al.*, 2008; *Conrad et al.*, 2007; *Martin-Short et al.*, 2015]. In subduction zone settings such as Alaska, where the mantle wedge is cooled and hydrated, B-type olivine LPO can develop, giving rise to a 90° change in the anisotropic fast direction, ϕ [*Karato et al.*, 2008]. A-type olivine LPO fabrics can also develop in the lithosphere in response to tectonic deformation [e.g., *Silver and Chan*, 1988; *Vauchez and Nicolas*, 1991; *Bastow et al.*, 2007; *Liddell et al.*, 2017; *De Plaen et al.*, 2014]. In addition to olivine LPO, the preferential alignment of fluid or melt [e.g. *Blackman and Kendall*, 1997; *Bastow et al.*, 2010], and the layering of rocks with different seismic velocities [*Backus*, 1962] can also impact the results of regional SKS splitting studies. Combinations of multiple mechanisms influence the observations in some regions [e.g., *Bastow et al.*, 2010; *Long and Becker*, 2010]. In the following sections, we explore each of these mechanisms as candidates to explain our Alaskan observations. In doing so, we pay close attention to whether or not asthenospheric flow is deflected at the edge of the subducting Pacific plate [*Eakin et al.*, 2009; *Mosher et al.*, 2014; *Paczkowski et al.*, 2014; *Jadamec and Billen*, 2010], and whether B-type olivine LPO is in evidence along an arc with variable slab-dip.

5.2 Seismic Anisotropy in Subduction Systems

At subduction zones, patterns in anisotropy may be extremely varied [e.g., *Long*, 2013; *Walpole et al.*, 2017] and shear-wave splitting observations can represent anisotropic contributions from the sub-slab mantle, the mantle wedge, the down-going slab and the overriding plate, making interpretations challenging [e.g., *Long and Silver*, 2008].

A simple model of viscous coupling between the downgoing slab and mantle beneath implies entrained mantle flow beneath the subducting slab, which would yield splitting fast directions perpendicular to the strike of the slab [*Long*, 2013]. However, shear-wave splitting studies [e.g. *Smith et al.*, 2001] have long indicated complex anisotropy patterns that cannot always be explained by such simple models. Previous observations at

©2018 American Geophysical Union. All rights reserved.

subduction zones worldwide reveal both slab-parallel and slab-perpendicular fast splitting directions and large variations in δt. Many subduction zones exhibit slab-parallel splitting, which is incompatible with simple entrainment models and has been variously attributed to three dimensional flow induced by trench rollback [e.g., *Long and Silver*, 2008], the transition from A-type to B-type olivine LPO in the relatively cool, hydrated nose of the mantle wedge [e.g., *Karato et al.*, 2008; *Kneller et al.*, 2005; *Ohuchi et al.*, 2012] or the effect of strong radial anisotropy within entrained flow that is steeply dipping [*Song and Kawakatsu*, 2012]. By studying patterns of anisotropy along ~40,000 km of the global subduction zone system, *Walpole et al.* [2017] found large variability in ϕ, noting that slab-parallel observations are only slightly more prominent than slab-perpendicular observations. *Walpole et al.* [2017] argue that slab-parallel shear-wave splitting can result from the strong radial anisotropy of asthenosphere entrained at steeply-dipping subduction zones, a view supported by the modeling work of *Song and Kawakatsu* [2012].

Geodynamic models show that the spatial extent of subduction-induced LPO and synthetic shear-wave splitting parameters can vary as a function of slab buoyancy and geometry [e.g. *Kneller and Van Keken*, 2007; *Faccenda and Capitanio*, 2013; *MacDougall et al.*, 2017]. In particular, *MacDougall et al.* [2017] show that the "zone of influence" of a subducting plate in the asthenosphere upon shear-wave splitting patterns changes with varying slab geometry. Studying the effect of varying slab dip on SKS splitting patterns, *Song and Kawakatsu* [2013] predict splitting fast directions that are sub-parallel to plate motion direction (i.e. trench-perpendicular) where the slab dip is small (5–10°). For a steeply dipping slab (≥40°), the predicted splitting fast directions are trench-parallel [*Song and Kawakatsu*, 2013]. By modeling the Mariana and Andean subduction zones, *Kneller and Van Keken* [2007] investigate the influence of the strong slab curvature and large along-strike variations in geometry. Modeling average Andean slab dips of 10–30°, they predict trench-perpendicular stretching in regions of shallow slab dip. Slab-parallel flow is predicted in the mantle wedge above the more steeply dipping slab region [*Kneller and Van Keken*, 2007]. Geodynamic models of slab-edge environments also predict the presence of toroidal flow of asthenospheric material around the side of slab from the underside into the mantle wedge [*Jadamec*, 2016]. This pattern of flow also has a component of upwelling, which is predicted to cause a concentration of null results in shear wave splitting studies [*Jadamec*, 2016].

Accepted Article

©2018 American Geophysical Union. All rights reserved.

Accepted Article

The pattern of shear-wave splitting results in our study region (Figure 6) features several abrupt shifts in fast directions that are consistent over long length scales (>200 km). This suggests several sources of anisotropy beneath different parts of Alaska, likely at different depths. Consistent measurements at nearby stations are indicative of large-scale layers of anisotropy, which we can link to tectonic processes. After comparing our results with previous splitting studies in the Alaska region in the following section, we discuss which mechanisms of anisotropy likely dominate across Alaska, and how they relate to studies at subduction systems elsewhere.

5.3 Comparison with Previous Studies in Alaska

Previous SKS splitting studies in Alaska have variously analyzed data from the permanent AK network, the temporary Broadband Experiment Across the Alaska Range (BEAAR), Alaska Receiving Cross Transect of the Inner Core (ARCTIC), and Multidisciplinary Observations Of Subduction (MOOS) networks [AK: *Hanna and Long*, 2012; BEAAR: *Christensen Abers*, 2009; BEAAR/ARCTIC/MOOS: *Perttu et al.,* 2014]. Our results corroborate previous work (Figure 7). Two main patterns of anisotropy emerge from these previous studies: slab-parallel fast directions indicative of along strike flow in the mantle wedge, and slab-perpendicular fast directions closer to the trench.

Hanna and Long [2012] argue that several factors contribute to their observed splitting pattern: shear in the asthenosphere due to absolute plate motion (APM), slab-parallel flow in the mantle wedge and two-dimensional entrained mantle flow beneath the slab. This corroborates the interpretations of *Perttu et al.* [2014] and *Christensen and Abers* [2009], who suggest that their observed splitting pattern is influenced mainly by: (i) along-strike asthenospheric flow in the mantle wedge where slab depth is >70 km and (ii) anisotropy within or below the subducting Pacific/Yakutat plate where the slab is shallower than 70 km.

5.4 Lithospheric Sources of Anisotropy

Anisotropy in the continental crust typically results in $\delta t = 0.1$–0.5 s [*Silver*, 1996; *Savage*, 1999; *Long*, 2009]. It is also largely uncorrelated with that of the underlying mantle [*Lin et al. 2011*]. Therefore, our δt values (mean $\delta t =$ 1.19 s) require a mantle con-

©2018 American Geophysical Union. All rights reserved.

tribution to the anisotropy. We calculate the splitting time produced by a vertical incident ray traveling through a single anisotropic layer of thickness L [*Silver and Chan*, 1991] as:

$$\delta t = \frac{\epsilon L}{\beta}, \tag{1}$$

where ϵ is the average % anisotropy, L is the anisotropic layer thickness, and β is shear-wave velocity. Using our observed mean δt = 1.19 s, β = 4.48 km/s [ak135 mantle velocities, *Kennett et al.*, 1995], and ϵ = 4% [upper estimate of the strength of anisotropy to 200 km depth, *Savage*, 1999], we find L = 133 km.

Some of our splitting parameters vary over short length scales. According to Fresnel zone arguments, this observation points towards a shallow source of anisotropy [e.g. *Alsina and Snieder*, 1995]. The length-scale of changes are in fact sometimes shorter than the width of the Fresnel zone at the base of the lithosphere (~125 km). A particularly dramatic change in ϕ is evident from slab-parallel north-west of the slab to slab-perpendicular closer to the trench where the subducting slab is shallower at stations such as CAPN, SSN or M22K (Figure 1). Beneath south-central Alaska, the Yakutat lithosphere subducts at a shallow angle until ~600 km inboard of the trench [e.g., *Eberhart-Phillips et al.*, 2006]. If there is alignment between fossil anisotropy in the continental lithosphere and underlying oceanic lithosphere, then the overall lithospheric contribution may be large at stations on the subducted Yakutat terrane, whose outline is indicated by the thick blue contour in Figure 6. We do not see evidence for a significant contribution to the splitting signal from other Alaskan terranes, however (Figure 1).

In the southeastern corner of our study area, fast directions parallel the direction of motion of the Fairweather and Queen Charlotte transform faults, a clear example of lithospheric anisotropy, whose development is ongoing. Our observations of delay times with an average of $\delta t = 1.19s$ can be compared to measurements along the San Andreas Fault to the south of our study area. The San Andreas is an archetypal example of a two-layer splitting case [*Silver and Savage*, 1994; *Polet and Kanamori*, 2002; *Özalaybey and Savage*, 1995]. In central and southern California, the splitting delay time associated with the upper, 'lithospheric' layer of San Andreas fault-parallel layer of anisotropy is considered relatively small (δt≤0.7 s), consistent with the region's thin lithosphere. Corroborating this hypothesis from a Fresnel zone point of view, stations to the west of the fault in southern/central California, show evidence for only a single layer of anisotropy, not associated

©2018 American Geophysical Union. All rights reserved.

Accepted Article

with the fault. In contrast, further north in California, a 115-125 km-thick layer of fault parallel anisotropy is observed *Özalaybey and Savage* [1995], akin to our results. We also observe that fast directions approximately parallel the Fairweather and Queen Charlotte transform faults up to ~100 km east of the fault, consistent with the hypothesis of a relatively thick lithospheric anisotropic layer (Figure 6). Away from the Fairweather and Queen Charlotte transform fault, alignment of fast polarization directions with structural trends are less clear. Thus, in the following sections we explore the role asthenospheric flow might play in governing our results.

5.5 Asthenospheric Sources of Anisotropy

5.5.1 Anisotropy Around the Slab Edge

The teleseismic body wave tomography study of *Martin-Short et al.* [2016] indicates a sharp slab edge beneath south central Alaska at ~145°W, 65°N (Figure 6). The splitting geometry appears to change across this feature, transitioning from a dominantly slab-parallel orientation west of slab edge to a fan-like pattern eastwards of the slab edge. The observed pattern of anisotropy east of the slab termination zone is similar to that predicted by the 3D instantaneous mantle flow models of toroidal flow around the Alaskan slab edge [*Jadamec and Billen*, 2010, 2012]. This flow geometry implies a decoupling of the sub-slab mantle and mantle wedge from the lithospheric plate motion [*Jadamec and Billen*, 2012]. However, our observations do not appear to match the model north-west of the slab, where we observe slab-parallel fast directions and the modelled flow predicts predominantly slab-normal fast directions. *Jadamec and Billen* [2010, 2012] also show that localized vertical upwelling occurs in the mantle near the WVF, for the preferred models using the SlabE115 slab geometry and buoyancy (Figure 8). This suggests that WVF volcanism may be in part driven by localized mantle upwelling upwelling associated with the toroidal asthenospheric flow around the edge of the Pacific-Yakutat slab [*Piromallo et al.*, 2006; *Strak and Schellart*, 2014; *Jadamec*, 2016]. The interpretation of our splitting observations as toroidal asthenospheric flow at the slab edge, in combination with the presence of a low velocity anomaly in the tomography beneath the WVF provides tentative evidence for the latter hypothesis for volcanism origin in the WVF.

The 3D flow around the slab edge appears to be competing with the influence of absolute plate motion (APM) as one moves further away from the trench, in the south-west

Accepted Article

©2018 American Geophysical Union. All rights reserved.

Accepted Article

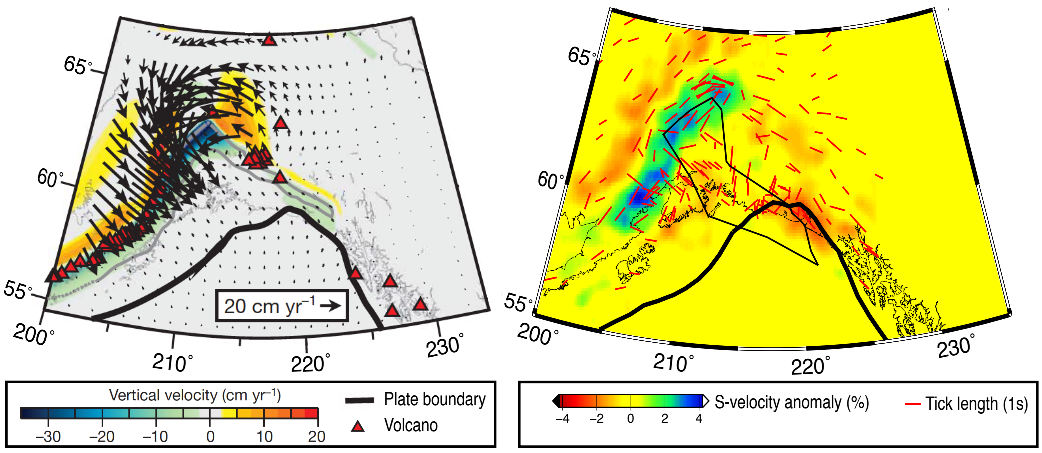

Figure 8. Comparison between the modeled mantle velocity field of *Jadamec and Billen* [2010] and our shear-wave splitting observations. Left: the velocity field at 100-km depth from an instantaneous flow model with composite viscosity (Figure from *Jadamec and Billen* [2010]). The displayed slab geometry slabE115 was preferred by *Jadamec and Billen* [2010] on the basis of a comparison between their modeled flow vectors and observed shear wave splitting results. Right: our SKS splitting observations overlain on a 200-km depth slice through the S-wave tomography model of *Martin-Short et al.* [2016]. A similar pattern of 3D flow around the north-east slab edge is observed in the instantaneous mantle flow field and the shear-wave splitting observations.

©2018 American Geophysical Union. All rights reserved.

Accepted Article

and northern-most regions of our study area. This is consistent with the flow field modelled by *Jadamec and Billen* [2010], suggesting a decrease in the magnitude of the slab edge-induced 3D flow away from the trench. However, due to variations in APM depending on the chosen model or reference frame (Figure 6), it is hard to determine the extent to which fast directions are aligned with APM away from the subduction zone. Thus, it is also challenging to determine the northern extent of the influence of slab-parallel flow induced by mantle flow around the slab edge. Geodynamic studies [e.g. *Piromallo et al.*, 2006; *Király et al.*, 2017] show that the generalized length scales of toroidal flow are in the range of 900-2000 km.

The dip of the down-going Pacific-Yakutat slab varies significantly along strike from nearly zero (flat slab subduction) below south-central Alaska to steeply dipping beyond 30°- 35°further west along the Aleutian-Alaska arc [*Eberhart-Phillips et al.*, 2006; *Song and Kawakatsu*, 2012; *Hayes et al.*, 2018]. The modeling work of *Kneller and Van Keken* [2007] has been shown that variations in slab dip and geometry along strike can result in a shift in splitting fast directions similar to that observed in our results immediately northwest of the slab. We therefore propose that in this region the near-vertical sinking of the arcuate slab with variable dip causes pressure gradients in the mantle wedge and the slab-parallel fast directions This process occurs in addition to the slab-parallel fast directions associated with toroidal flow that occurs around the northern tip and eastern slab edge [e.g. *Jadamec and Billen*, 2010, 2012]. We also cannot preclude the possibility that slab depth might also be a controlling factor to the mantle flow pattern, as modeled by *Lin* [2014] in the Chilean subduction zone.

Tian and Zhao [2012] produced a tomographic model of P-wave velocities and anisotropy from local earthquakes, at depths of ≤190 km beneath south central Alaska. They also argue for a similar flow around the slab edge driven by a varied slab geometry a long strike that yields slab-parallel fast directions in the mantle wedge and sub-slab mantle. However, their interpretation includes the presence of a significant "Wrangell" slab east of the slab imaged by *Martin-Short et al.* [2016]. *Jadamec and Billen* [2010, 2012] developed and tested two slab geometries for the Alaska-Wrangell slab, one with a deeper Wrangell slab segment (SlabE325) and another with a shorter Wrangell slab (SlabE115). The flow field associated with the preferred model in *Jadamec and Billen* [2010, 2012] using SlabE115 appears much more similar to our shear-wave splitting observations than that associated with a geometry featuring deep suduction beneath the WVF. This supports the interpreta-

©2018 American Geophysical Union. All rights reserved.

tion of *Martin-Short et al.* [2016] with regard to WVF subduction and lends credence to the idea that the observed toroidal splitting pattern is caused by flow around a truncated Pacific-Yakutat slab beneath south-central Alaska.

5.5.2 Slab-Perpendicular Anisotropy

One of the most striking and consistent features of our results is the transition from slab-perpendicular to slab-parallel splitting directions northwestwards across the slab (in the northeastern-most part of the delimited Yakutat terrane delimited in Figure 6.). The shift in dominant influence from slab-parallel flow in the mantle wedge to the combination of sub-slab entrained flow and lithospheric anisotropy in the Yakutat terrane could explain the dramatic contrast in splitting directions that occurs across small length scales (<100 km).

Splitting measurements from stations west of the volcanic arc and Denali Volcanic Gap appear to follow southwestwards the curvature of the downgoing slab as constrained from the tomography of *Martin-Short et al.* [2016], which suggests a steeply dipping slab at great depths (>200 km) in this region. This implies that the mantle wedge is sufficiently thick to provide a source of anisotropy capable of producing the observed delay times. Thus, we suggest that these slab-parallel results are caused mainly by asthenospheric flow in the mantle wedge along the strike of the slab.

Slab-perpendicular results around stations such as CAPN and M22K are consistent with the study of *Hanna and Long* [2012] (Figure 6). These authors argue that a sub-slab layer of entrained asthenosphere is responsible for this pattern; an interpretation that is consistent with splitting observations at other zones of shallow subduction *Long and Silver* [2009]. East of the volcanic arc, where the Yakutat terrane is subducting, the mantle wedge is thin (<100 km) and the dip of the subducting lithosphere is relatively shallow due to the presence of thick Yakutat crust. Thus the main asthenospheric source of anisotropy is the sub-slab mantle. We suggest that the slab-perpendicular splitting results may be caused by a thick asthenospheric layer entrained beneath the downgoing Yakutat slab. The slab-perpendicular measurements can therefore be interpreted as resulting from a combination of lithospheric (fossil anisotropy within the subducting Yakutat) and asthenospheric (sub-slab mantle entrained by the drag of the subducting plate) sources.

Accepted Article

©2018 American Geophysical Union. All rights reserved.

Several stations above the subducted Yakutat terrane (e.g. KLU, BMR) display a consistent, N-S orientated splitting pattern (Figure 6). This may be the result of entrained asthenospheric flow beneath the Yakutat lithosphere, a particularly thick or highly anisotropic section of Yakutat lithosphere itself, or by alignment of fossil anisotropy directions within the Yakutat and overlying continental lithosphere. There is a notable change in splitting geometry between this N-S orientated pattern south of the WVF and a predominantly SE-NW orientated pattern to the north. If the N-S orientated pattern is related to the presence of Yakutat lithosphere, then this abrupt change implies that subduced Yakutat lithosphere is not present to the north of the WVF. Thus these volcanoes may have formed at a slab edge, which is a conclusion supported by the imaging work of *Martin-Short et al.* [2018].

Figure 9 illustrates the main conclusions from our study showing the processes driving seismic anisotropy at the Alaskan subduction zone.

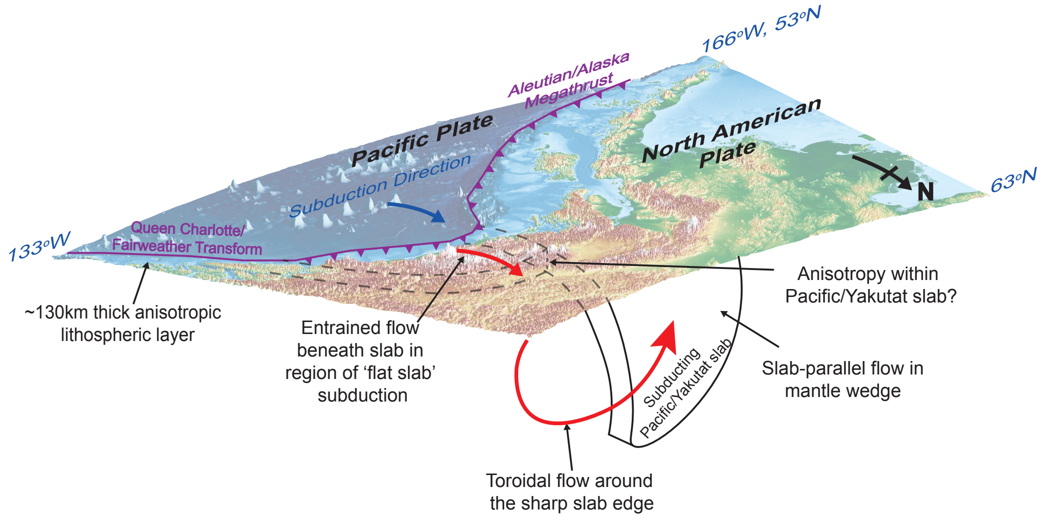

Figure 9. Summary sketch of mechanisms driving anisotropy in Alaska.

©2018 American Geophysical Union. All rights reserved.

Accepted Article

Accepted Article

6 Conclusions

We have performed a shear-wave splitting study of upper mantle anisotropy in south-central Alaska using data from a large collection of seismic networks, including the Transportable Array (TA). In doing so, we place new constraints on the tectonics and mantle geodynamics at the south-central Alaskan subduction margin. Anisotropic fast directions (ϕ) vary over short length scales (~50 km) suggesting relatively shallow sources of seismic anisotropy in some areas. For example, in the vicinity of the Queen Charlotte and Fairweather transform faults, ϕ parallels these faults, consistent with a lithospheric source of anisotropy. However, the high delay times (δt = 1–1.5 s) obtained across the study region require an asthenospheric contribution to the anisotropic signal. We develop our interpretations using both shear-wave splitting observations and an S-wave tomography model of Alaska. The pattern of fast directions wrapping around the slab edge implies a three-dimensional toroidal mantle flow in this area 9. Upwelling at the slab edge associated with this asthenospheric flow may thus be the cause of volcanism in the Wrangell Volcanic Field (*Jadamec and Billen*, 2010, 2012). Closer to the trench, we observe a 90°rotation in ϕ from slab-parallel to slab-perpendicular, correlating with the location of the Yakutat terrane. This dramatic change in fast directions across the Yakutat subduction region can be interpreted as resulting from the influence of fossil lithospheric anisotropy within the Yakukat terrane, supported by the imaging work of *Martin-Short et al.* [2018] and by the geodynamic modeling of *Jadamec and Billen*, [2010, 2012]. However, high delay times obtained across the Yakutat region (δt≈1.5 s) also suggest entrained sub-slab mantle flow as an anisotropic source. Ultimately, we infer that that variability in slab geometry exerts first order control on the pattern of mantle flow in south-central Alaska.

Acknowledgments

The facilities of IRIS Data Services, and specifically the IRIS Data Management Center, were used for access to waveforms, related metadata, and/or derived products used in this study. IRIS Data Services are funded through the Seismological Facilities for the Advancement of Geoscience and EarthScope (SAGE) Proposal of the National Science Foundation under Cooperative Agreement EAR-1261681. Data from the AK network was made available by the University of Alaska Fairbanks (Alaska Earthquake Center, Univ. of Alaska Fairbanks (1987): Alaska Regional Network. International Federation of Digi-

©2018 American Geophysical Union. All rights reserved.

Accepted Article

tal Seismograph Networks. 10.7914/SN/AK.) and data for the AT network by the NOAA National Oceanic and Atmospheric Administration (NOAA National Oceanic and Atmospheric Administration (USA) (1967): National Tsunami Warning Center Alaska Seismic Network. International Federation of Digital Seismograph Networks. doi:10.7914/SN/AT). Data from the TA network (IRIS Transportable Array (2003): USArray Transportable Array. International Federation of Digital Seismograph Networks. 10.7914/SN/TA) were made freely available as part of the EarthScope USArray facility, operated by Incorporated Research Institutions for Seismology (IRIS) and supported by the National Science Foundation, under Cooperative Agreements EAR-1261681. Figures in this article were made using the Generic Mapping tools [*Wessel et al.*, 2013] and the Python Matplotlib library. The paper benefited from discussions with B. Romanowicz and W. Hawley.

References

Alaska Earthquake Center, Univ. of Alaska Fairbanks (1987): Alaska Regional Network. International Federation of Digital Seismograph Networks. doi:10.7914/SN/AK.

Alsina, D. and Snieder, R. (1995). Small-scale sublithospheric continental mantle deformation: constraints from SKS splitting observations. *Geophys. J. Int.*, *123*, 431–448. doi:10.1111/j.1365-246X.1995.tb06864.

Backus, G. E. (1962). Long-wave elastic anisotropy produced by horizontal layering. *J. Geophys. Res.*, *67*(11), doi:10.1029/JZ067i011p04427.

Bastow, I. D., Owens, T. J., Helffrich, G. and Knapp, J. H. (2007). Spatial and temporal constraints on sources of seismic anisotropy: Evidence from the Scottish highlands. *Geophys. Res. Lett.*, *34*. doi:10.1029/2006GL028911.

Bastow, I. D., Pilidou, S., Kendall, J.-M., and Stuart, G. (2010). Melt-induced seismic anisotropy and magma assisted rifting in Ethiopia: evidence from surface waves. *Geochem. Geophys. Geosyst.*, *11*, Q0AB05. doi:10.1029/2010GC003036.

Bird, P. (2003), An updated digital model of plate boundaries, *Geochem. Geophys. Geosyst.*, *4*(3), doi:10.1029/2001GC000252.

Blackman, D., and J.-M. Kendall (1997). Sensitivity of teleseismic body waves to 635 mineral texture and melt in the mantle beneath a mid-ocean ridge. *Phil. Trans. R. Soc. Lond.*, 355, 217–231.

Bokelmann, G., and Silver, P. (2002). Shear stress at the base of shield lithosphere. *Geophys. Res. Lett.*, *29*(23). doi:10.1029/2002GL015925.

©2018 American Geophysical Union. All rights reserved.

Accepted Article

Brueseke, M. E., Benowitz, J.A., Trop, J.M., Davis, K.N., Berkelhammer, S.E., Layer, P.W. and Morter, B.K. (2019). The Alaska Wrangell Arc: ~30 Ma of subduction-related magmatism along a still active arc-transform junction. *Terra Nova*, *31*(1), doi.org/10.1111/ter.12369.

Christensen, D.H. and Abers, G.A. (2009). Seismic anisotropy under central Alaska from SKS splitting observations. *J. Geophys. Res.*, *115*, B04315. doi:10.1029/2009JB006712.

Christenson, G. L., Gulick, S. P. S., van Avendonk, H. J. A., Worthington, L. L., Reece, R. S. and Pavlis, T. L. (2010). The Yakutat terrane: Dramatic change in crustal thickness across the Transition fault, Alaska. *Geology*, *38*(10), 895–898.

Colpron, M., Nelson, J. L. and Murphy, D. C. (2007). Northern Cordilleran terranes and their interactions through time. *GSA Today*, *17*, doi:10.1130/GSAT01704-5A.1.

Conrad, C.P., Behn, M.D. and Silver, P.G. (2007). Global mantle flow and the development of seismic anisotropy: Differences between the oceanic and continental upper mantle. *J. Geophys. Res.*, *112*, doi:10.1029/2006JB004608.

Darbyshire, F.A., Bastow, I.D., Forte, A.M., Hobbs, T.E., Calvel, A., Gonzalez-Monteza, A. and Schow, B. (2015). Variability and origin of seismic anisotropy across eastern Canada: Evidence from shear-wave splitting measurements. *J. Geophys. Res.*. doi: 10.1002/2015JB012228.

De Plaen, R., I. Bastow, E. Chambers, D. Keir, R. Gallacher, and J. Keane (2014), The development of magmatism along the Cameroon Volcanic Line: Evidence from seismicity and seismic anisotropy, *J. Geophys. Res.*, *119*, 4233–4252, doi: 10.1002/2013JB010583.

Eakin C.M., Obrebski, M., Allen, R.M., Boyarko, D.C., Brudzinski, M.R. and Porritt, R. (2009). Seismic anisotropy beneath Cascadia and Mendocino triple junction: Interaction of the subducting slab with mantle flow. *Earth Planet. Sci. Letts.*, *297*, 627–632. doi: 10.1016/j.epsl.2010.07.015.

Eberhart-Phillips, D., Christensen, D. H., Brocher, T. M., Hansen, R., Ruppert, N. A., Haeussler, P. J. and Abers, G.A. (2006). Imaging the transition from Aleutian subduction to Yakutat collision in central Alaska, with local earthquakes and active source data. *J. Geophys. Res.*, *111*, B11303. doi:10.1029/2005JB004240.

Faccenda, M. and Capitanio, F.A. (2013). Seismic anisotropy around subduction zones: Insights from three-dimensional modeling of upper mantle deformation and SKS splitting calculations. *Geochem. Geophys. Geosyst.*, 14(1), 243–262.

©2018 American Geophysical Union. All rights reserved.

Accepted Article

Ferris, A., Abers, G. A., Christensen, D. H. and Veenstra, E. (2003). High resolution image of the subducted Pacific (?) plate beneath central Alaska, 50–150 km depth. *Earth Planet. Sci. Lett.*, *214*(3–4), 575-588.

Finzel, E. S., Trop, J. M., Ridgway, K. D. and Enkelmann, E. (2011). Upper plate proxies for flat-slab subduction processes in southern Alaska. *Earth Planet. Sci. Lett.*, 303(3–4), 348–360.

Finzel, E. S., Flesch, L.M., Ridgway, K.D., Holt, W.E. and Ghosh, A. (2015). Surface motions and intraplate continental deformation in Alaska driven by mantle flow *Geophys. Res. Lett.* , *42*, 4350–4358, doi:10.1002/2015GL063987.

Gilligan, A., Bastow, I. D., Watson, E., Darbyshire, F. A., Levin, V., Menke, W., Lane, V., Hawthorn, D., Boyce, A., Liddell, M.V. and Petrescu, L. (2016). Lithospheric deformation in the Canadian Appalachians: evidence from shear-wave splitting. *Geophys. Jour. Int.*, *206*, 1273–1280.

Gripp, A. and Gordon, R. (2002). Young tracks of hotspots and current plate velocities. *Geophys. J. Int.*, *150*, 321–361.

Hall, C. E., Fisher, K. M. and Parmentier, E.M. (2000). The influence of plate motions on three-dimensional back arc mantle flow and shear-wave splitting. *J. Geophys. Res.*, *105*(B12), 28,009–28,033.

Hanna, J., and Long, M. (2012). SKS splitting beneath Alaska: Regional variability and implications for subduction processes at a slab edge. *Tectonophysics*, *530–531*, 272–285, doi:10.1016/j.tecto.2012.01.003.

Hayes, G.P., Moore, G.L., Portner, D.E., Hearne, M., Flamme, H., Furtney, M., Smoczyk, G.M. (2018). Slab2, a comprehensive subduction zone geometry model. *Science*, *362*, 6410, 58–61 doi:10.1126/science.aat4723.

Holtzman, B.K. and Kendall, J-M. (2010). Organized melt, seismic anisotropy, and plate boundary lubrication. *Geochem. Geophys. Geosyst.*, *11*, doi:10.1029/2010GC003296.

IRIS Transportable Array (2003): USArray Transportable Array. International Federation of Digital Seismograph Networks. Other/Seismic Network. doi:10.7914/SN/TA.

Jadamec, M. A. and Billen, M. I. (2010). Reconciling surface plate motions with rapid three-dimensional mantle flow around a slab edge. *Nature*, *465*, doi: 10.1038/nature09053.

Jadamec, M. A., and Billen, M.I. (2012). The role of rheology and slab shape on rapid mantle flow: Three-dimensional numerical models of the Alaska slab edge. *J. Geophys.*

©2018 American Geophysical Union. All rights reserved.

Res., 117, B02304, doi:10.1029/2011JB008563.

Jadamec, M. A., Billen, M.I. and Roeske, S.M. (2013). Three-dimensional numerical models of flat slab subduction and the Denali fault driving deformation in south-central Alaska. *Earth Planet. Sci. Lett.*, 376, 29–42, doi:10.1016/j.epsl.2013.06.009.

Jadamec, M. A. (2016). Insights on slab-driven mantle flow from advances in three-dimensional modelling. *J. Geodyn.*, *100*, 51–70, doi:10.1016/j.jog.2016.07.004.

Karato, S., Jung, H., Katayama, I. and Skemer, P. (2008). Geodynamic Significance of Seismic Anisotropy of the Upper Mantle: New Insights from Laboratory Studies. *Annu. Rev. Earth Planet. Sci.*, *36*, 59–95, doi:10.1146/annurev.earth.36.031207.124120.

Kennett, B. L. N., Engdahl, E. R. and Buland, R. (1995). Constraints on seismic velocities in the Earth from traveltimes. *Geophys. J. Int.*, *122*, 108–124.

Király, A., Capitanio, F.A., Funiciello, F., Faccenna, C. (2017). Subduction induced mantle flow: Length-scales and orientation of the toroidal cell. *Earth Planet. Sci. Lett.*, *479*, 284–297.

Kneller, E., Van Keken, P., Karato, S., and Park, J. (2005). B-type olivine fabric in the mantle wedge: Insights from high-resolution non-Newtonian subduction zone models. *Earth Planet. Sci. Lett.*, 237(3–4), 781–797.

Kneller, E., and P. Van Keken (2007), Trench-parallel flow and seismic anisotropy in the Mariana and Andean subduction systems, *Nature*, *450*(7173), 1222.

Koons, P.O., Hooks, B.P., Pavlis, T., Upton, P. and Barker, A.D. (2010), Three-dimensional mechanics of Yakutat convergence in the southern Alaskan plate corner, *Tectonics*, *29*, TC4008, doi:10.1029/2009TC002463.

Liddell, M., Bastow, I.D., Darbyshire, F.A., Gilligan, A. and Pugh. S. (2010). The formation of Laurentia: Evidence from shear-wave splitting. *Earth Planet. Sci. Lett.*, *479*, 170–178.

Lin, F-C et al. (2011). Complex and variable crustal and uppermost mantle seismic anisotropy in the western United States. *Nature Geoscience*. *4*, 55.

Lin, S.-C. (2014). Three-dimensional mantle circulations and lateral slab deformation in the southern Chilean subduction zone. *J. Geophys. Res.* 119(4), 3879–3896.

Long, M., and Silver, P. (2008). The Subduction Zone Flow Field from Seismic Anisotropy: A Global View. *Science*, *319*(5861), 315–318. doi: 10.1126/science.1150809.

©2018 American Geophysical Union. All rights reserved.

Long, M., and Silver, P. (2009). Shear-Wave Splitting and Mantle Anisotropy: Measurements, Interpretations, and New Directions. *Surveys in Geophysics*, 30(4), 407–461.

Long, M., and Becker, T.W. (2010). Mantle dynamics and seismic anisotropy *Earth Planet. Sci. Lett.*, *297*, 341–354. doi:10.1016/j.epsl.2010.06.036.

Long, M. (2013). Constraints on subduction geodynamics from seismic anisotropy. *Rev. Geophys.*, *51*, 76–112. doi:10.1002/rog.20008.

MacDougall, J.G., Jadamec, M.A. and Fisher, K.M. (2017). The zone of influence of the subducting slab in the asthenospheric mantle. *J. Geophys. Res. Solid Earth*, *122*, 6599-6624.

Martin-Short, R., Allen, R.M., Bastow, I.D., Totten, E. and Richards, M.A., (2015). Mantle flow geometry from ridge to trench beneath the Gorda-Juan de Fuca plate system. *Nat. Geosci.*, *8*, 965–968. doi:10.1038/ngeo2569.

Martin-Short, R., Allen, R.M. and Bastow, I.D. (2016). Subduction geometry beneath south central Alaska and its relationship to volcanism. *Geophys. Res. Lett.*, *43*. doi: 10.1002/2016GL070508.

Martin-Short Robert, et al. (2018). Seismic Imaging of the Alaska Subduction Zone: Implications for Slab Geometry and Volcanism. *Geochemistry, Geophysics, Geosystems*.

Moore, T.E. and Box, S.E. (2016). Age, distribution and style of deformation in Alaska north of 60°N: Implications for assembly of Alaska *Tectonophysics*, *691*(A), 133–170 doi:10.1016/j.tecto.2016.06.025.

Mosher, S.G., Audet, P. and L'Heureux, I. (2014). Seismic evidence for rotating mantle flow around subducting slab edge associated with oceanic microplate fracture. *Geophys. Res. Lett.*, *41*(13), 4548–4553. doi:10.1002/2014GL060630.

NOAA National Oceanic and Atmospheric Administration (USA) (1967): National Tsunami Warning Center Alaska Seismic Network. International Federation of Digital Seismograph Networks. Other/Seismic Network. doi:10.7914/SN/AT.

Nokleberg, W. J., Parfenov, L. M., Monger, J. W. H., Norton, I. O., Khanchuk, A. I., Stone, D. B., Scotese, C. R., Scholl, D. W. and Fujita, K. (2000). Phanerozoic tectonic evolution of the circum-North Pacific. *U.S. Geol. Surv. Prof. Pap.*, 1626, 122.

Nye, C. (1999). The Denali volcanic gap — Magmatism at the eastern end of the Aleutian arc. *Eos Tran. AGU*, *80*(46), Fall Meet. Suppl., 1203.

O'Driscoll, L. J., and Miller, M.S. (2015). Lithospheric discontinuity structure in Alaska, thickness variations determined by Sp receiver functions. *Tectonics*, *34*(4), 694–714.

Accepted Article

©2018 American Geophysical Union. All rights reserved.

Accepted Article

Ohuchi, T., Kawazoe, T., Nishihara, Y. and Irifune, T. (2012). Change of olivine a-axis alignment induced by water: Origin of seismic anisotropy in subduction zones. *Earth Planet. Sci. Lett.*, 317-318, 111–119.

Özalaybey, S., and M. Savage (1995), Shear-wave splitting beneath western United States in relation to plate tectonics, *J. Geophys. Res.*, *100*(B9), 18,135–18,149.

Paczkowski, K., Thissen, C.J., Long, M.D., and Montési, L.G.J. (2014). Deflection of mantle flow beneath subducting slabs and the origin of subslab anisotropy. *Geophys. Res. Lett.*, *41*, doi:10.1002/ 2014GL060914.

Perttu, A., Christensen, D., Abers, G., and Song, X. (2014). Insights into mantle structure and flow beneath Alaska based on a decade of observations of shear-wave splitting. *J. Geophys. Res.*, *119*(11), 8366–8377.

Piromallo, C., Becker, T.W., Funiciello, F., Faccenna, C. (2006). Three-dimensional instantaneous mantle flow induced by subduction. *Geophys. Res. Lett.*, *33*, L08304, doi: 10.1029/2005GL025390.

Plafker, G. and Berg, H. (1994). Overview of the geology and tectonic evolution of Alaska, in The Geology of North America, *G-1*, 389–449, eds. Plafker, G. and Berg, H., *Geol. Soc. Am.*, Boulder, CO.

Polet, J. and Kanamori, H. (2002). Anisotropy beneath California: shear wave splitting measurements using a dense broadband array. *Geophys. J. Int.*, 149(2), 313–327

Preece, S.J. and Hart, W.K. (2004). Geochemical variations in the < 5 Ma Wrangell Volcanic Field, Alaska: implications for the magmatic and tectonic development of a complex continental arc system. *Tectonophysics*, 392(1-4), 165–191.

Qi, C., Zhao, D., and Chen, Y. (2007). Search for deep slab segments under Alaska. *Phys. Earth Planet. Inter.*, *165*(1–2), 68–82.

Richter, D.H., Smith, J.G., Lanphere, M.A., Dalrymple, G.B., Reed, B.L. and Shew, N. (1990). Age and progression of volcanism, Wrangell volcanic field, Alaska. *Bull. Volcanol.*, 53(1), 29–44.

Rondenay, S., Montesi, L.G.J. and Abers, G.A. (2010). New geophysical insight into the origin of the Denali volcanic gap. *Geophys. J. Int.*, *182*(2), 613–630.

Savage, M. and Silver, P. (1993). Mantle deformation and tectonics: constraints from seismic anisotropy in the western United States. *Phys. Earth Planet. Int.*, *78*, 207–227.

Savage, M.K. (1999). Seismic anisotropy and mantle deformation: what have we learned from shear-waves. *Rev. Geophys.*, *37*(1), 65–106.

©2018 American Geophysical Union. All rights reserved.

Sauber, J., McClusky, S. and King, R. (1997). Relation of ongoing deformation rates to the subduction zone process in southern Alaska. *Geophys, Res. Lett.*, *24*, 2853–2856.

Silver, P., and Chan, W. (1988). Implications for continental structure and evolution from seismic anisotropy. *Nature*, *335*, 6185, doi:10.1038/335034a0.

Silver, P.G. and Chan, W.W. (1991). Shear-wave splitting and subcontinental mantle deformation, *J. Geophys. Res.*, *96*, 429–454.

Silver, P., and M. Savage (1994), The interpretation of shear wave splitting parameters in the presence of two anisotropic layers, *Geophys. J. Int.*, *119*, 949–963.

Silver, P.G. (1996). Seismic anisotropy beneath the continents: probing the depths of geology. *Nature*, *335*, 15303-15318.

Smith G.P., Wiens, D.A., Fisher, K.M., Dorman, L.M., Webb, S.C. and Hildebrand, J.A. (2001). A complex pattern of mantle flow in the Lau Backarc *Science*, *292*, 713–716, doi:10.1126/science.1058763.

Song, T., and Kawakatsu, H. (2012). Subduction of oceanic asthenosphere: evidence from sub-slab seismic anisotropy. *Geophys. Res. Lett.*, *39*(17), doi:10.1029/2012GL052639.

Song, T., and Kawakatsu, H. (2013). Subduction of oceanic lithospheric: A critical appraisal in central Alaska. *Earth Planet. Sci. Lett.*, 367, 82–94.

Strak, V. and Schellart, W.P. (2014). Evolution of 3-D subduction-induced mantle flow around lateral slab edges in analogue models of free subduction analysed by stereoscopic particle image velocimetry technique. *Earth Planet. Sci. Lett.*, 403, 368–379.

Teanby, N., J.-M. Kendall, and M. Van der Baan (2004), Automation of shear-wave splitting measurements using cluster analysis, *Bull. Seis. Soc. Am.*, *94*(2), 453–463, doi: 10.1785/0120030123.

Tian, Y., and Zhao, D. (2012). P-wave tomography of the western United States: Insight into the Yellowstone hotspot and the Juan de Fuca slab. *Phys. Earth Planet. Int.*, *200*, 72–84.

Vauchez, A., and Nicolas, A. (1991). Mountain building: strike-parallel motion and mantle anisotropy. *Tectonophysics*, *185*(3–4), 183–201.

Walpole, J., Wookey, J., Kendall, J.-M. and T.-G. Masters (2017). Seismic anisotropy and mantle flow below subducting slabs. *Earth Planet. Sci. Lett.*, 465, 155–167.

Wang, Y. and Tape, C. (2014). Seismic velocity structure and anisotropy of the Alaska subduction zone based on surface wave tomography. *J. Geophys. Res.*, *119*, 8845–8865, doi:10.1002/2014/JB011438.

Accepted Article

©2018 American Geophysical Union. All rights reserved.

Wessel, P., Smith, W. H. F., Scharroo, R., Luis, J. F. and Wobbe, F. (2013). Generic Mapping Tools: Improved version released. *EOS Trans. AGU*, *94*, 409-410.

Wolfe, C.J. and Silver, P.G. (1998). Seismic Anisotropy of oceanic upper mantle: Shear-wave splitting methodologies and observations. *J. Geophys. Res.*, *103*, 749–771.

Worthington, L.L., Van Avendonk, H.J.A., Gulick, S.P.S., Christeson, G.L., and Pavlis, T.L. (2012). Crustal structure of the Yakutat terrane and the evolution of subduction and collision in southern Alaska. *J. Geophys. Res.*, *117*, B01102, doi: 10.1029/2011JB008493.

Zhang, S. and Karato, S., (1995). Lattice preferred orientation of olivine aggregates deformed in simple shear. *Nature*, *375*, 774–777. doi:10.1038/375774a0.

Accepted Article

©2018 American Geophysical Union. All rights reserved.

Figure1.

Accepted Article

©2018 American Geophysical Union. All rights reserved.

Accepted Article

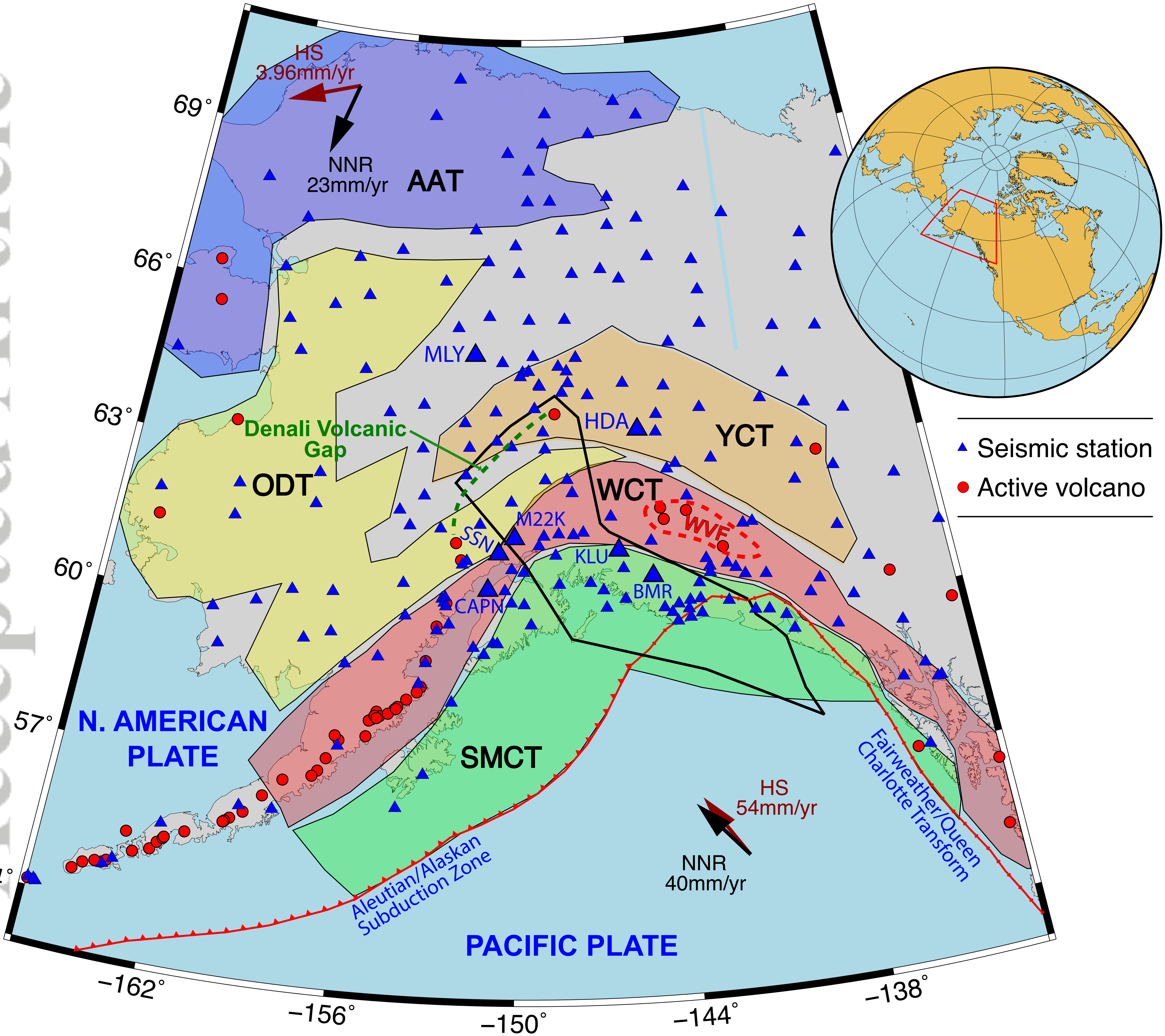

©2018 American Geophysical Union. All rights reserved.

Figure2.

Accepted Article

©2018 American Geophysical Union. All rights reserved.

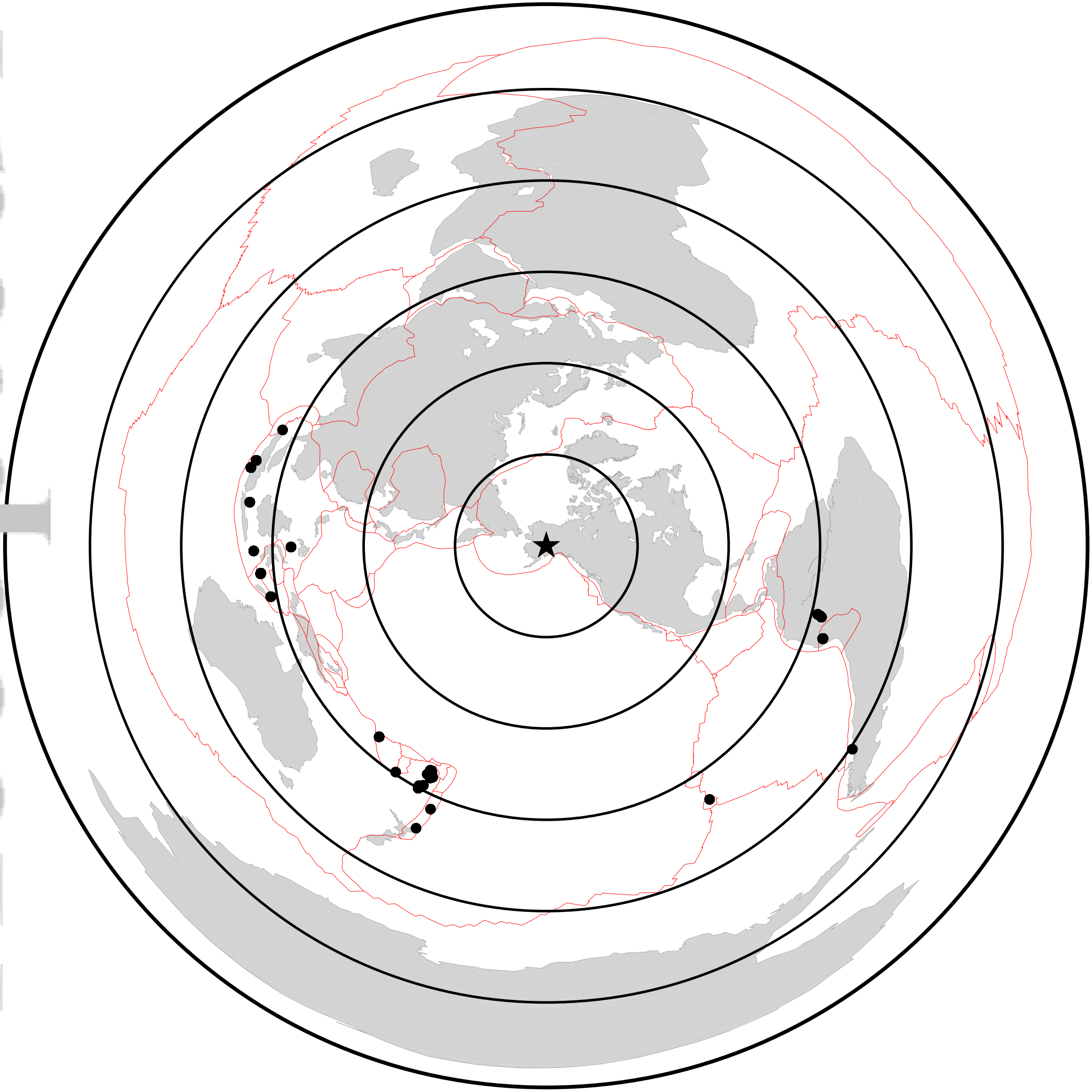

Figure3.

Accepted Article

©2018 American Geophysical Union. All rights reserved.

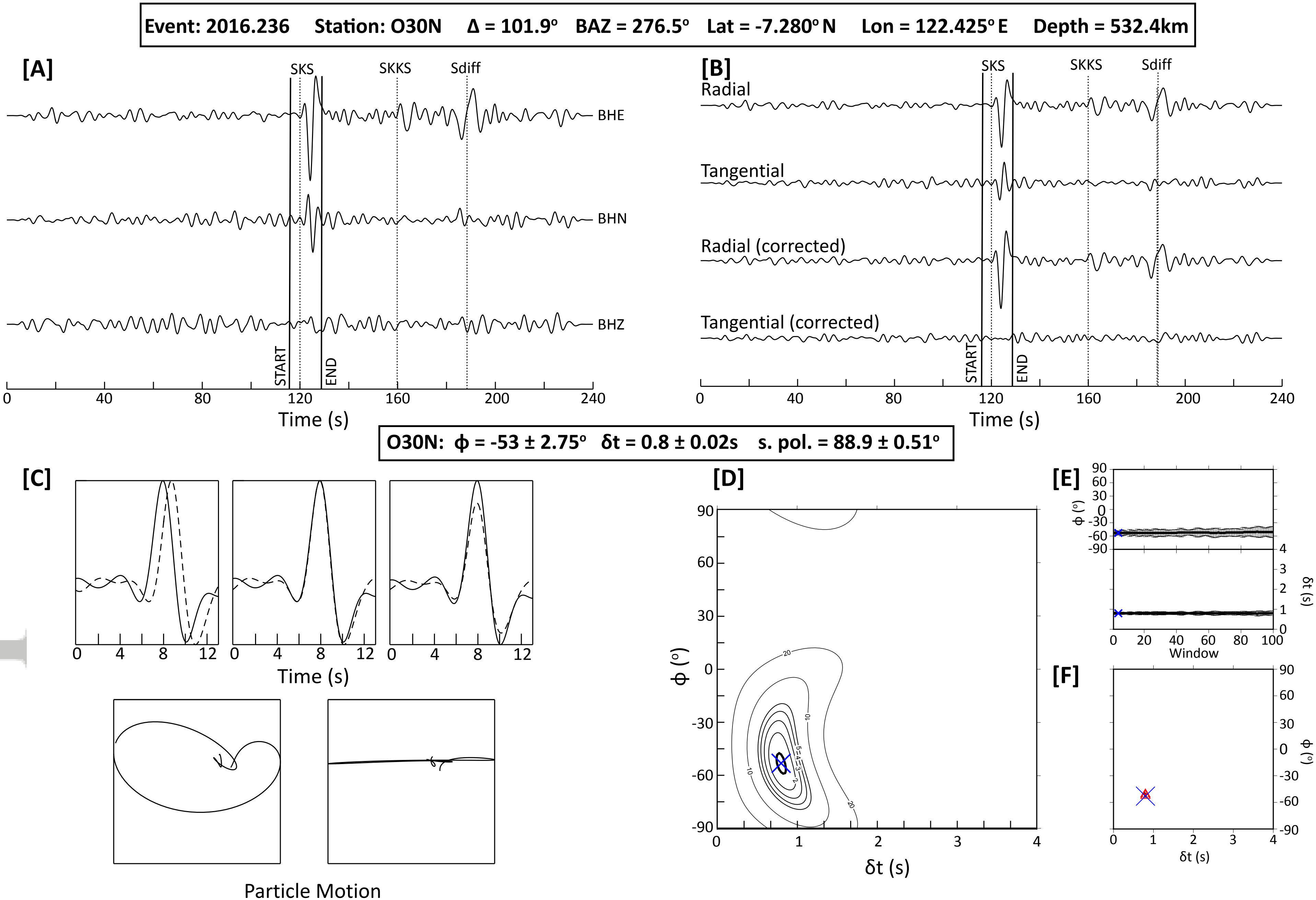
Event: 2016.236 Station: O30N Δ = 101.9° BAZ = 276.5° Lat = -7.280° N Lon = 122.425° E Depth = 532.4km
[A]
SKS
SKKS
Sdiff
BHE
BHN
BHZ
START
END
Time (s)
[B]
Radial
Tangential
Radial (corrected)
Tangential (corrected)
Time (s)
O30N: ϕ = -53 ± 2.75° δt = 0.8 ± 0.02s s. pol. = 88.9 ± 0.51°
[C]
Time (s)
Particle Motion
[D]
ϕ (°)
δt (s)
[E]
ϕ (°)
δt (s)
Window
[F]
δt (s)
ϕ (°)

Figure4.

Accepted Article

©2018 American Geophysical Union. All rights reserved.

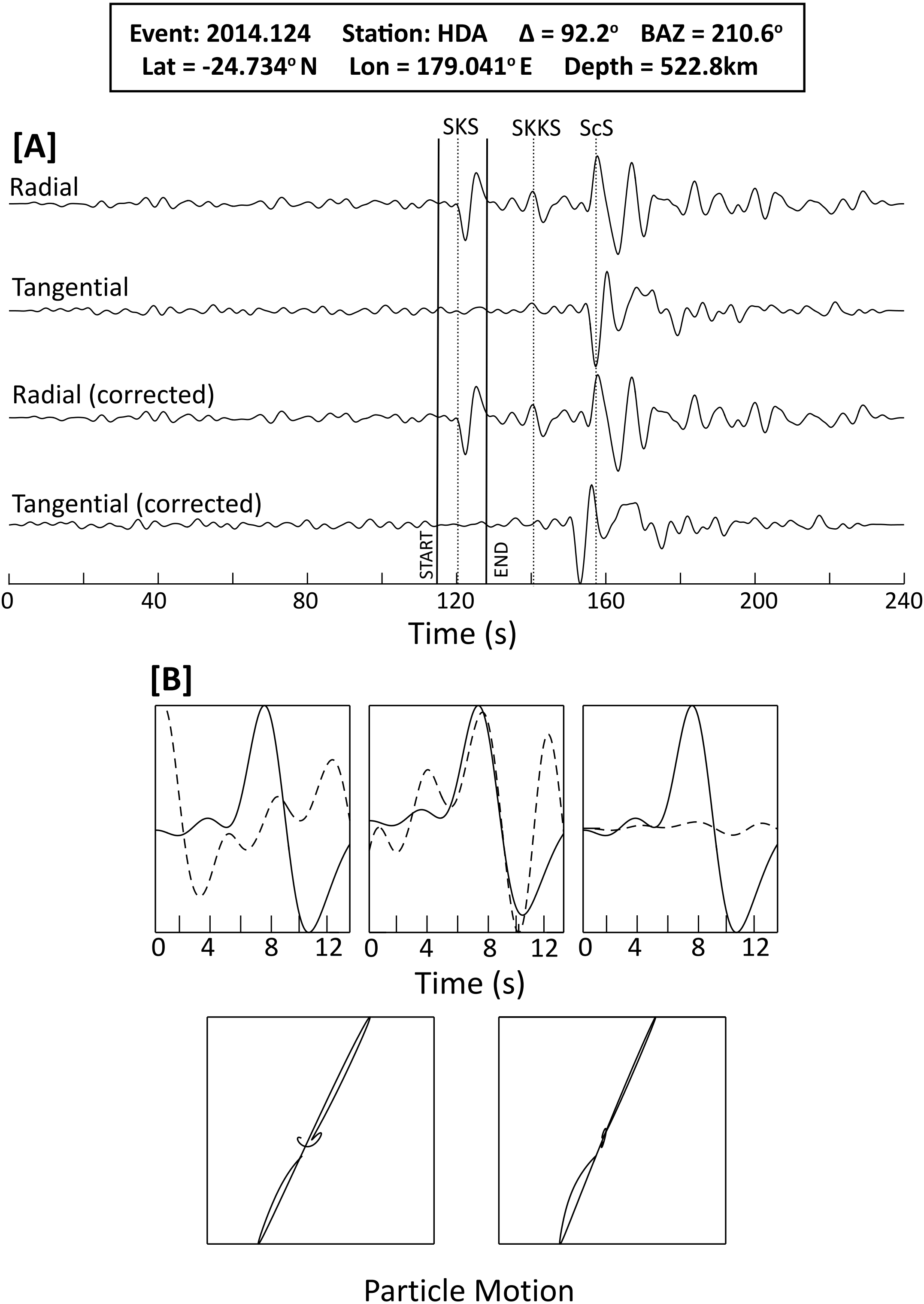

Event: 2014.124 Station: HDA Δ = 92.2° BAZ = 210.6°
Lat = -24.734° N Lon = 179.041° E Depth = 522.8km
[A]
SKS
SKKS
ScS
Radial
Tangential
Radial (corrected)
Tangential (corrected)
START
END
0
40
80
120
160
200
240
Time (s)
[B]
0
4
8
12
Time (s)
Particle Motion

Figure5.

Accepted Article

©2018 American Geophysical Union. All rights reserved.

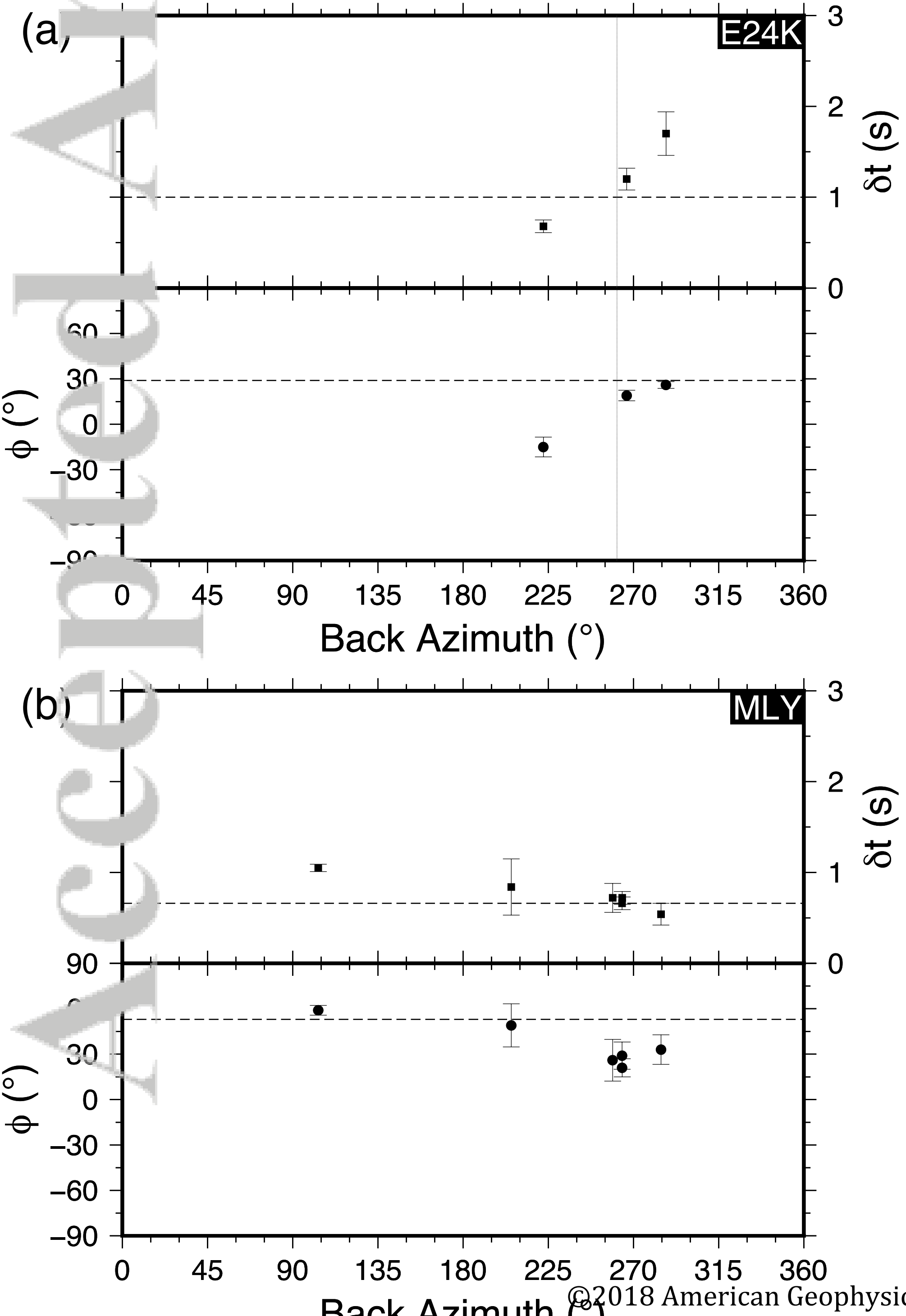

©2018 American Geophysic

Figure6.

Accepted Article

©2018 American Geophysical Union. All rights reserved.

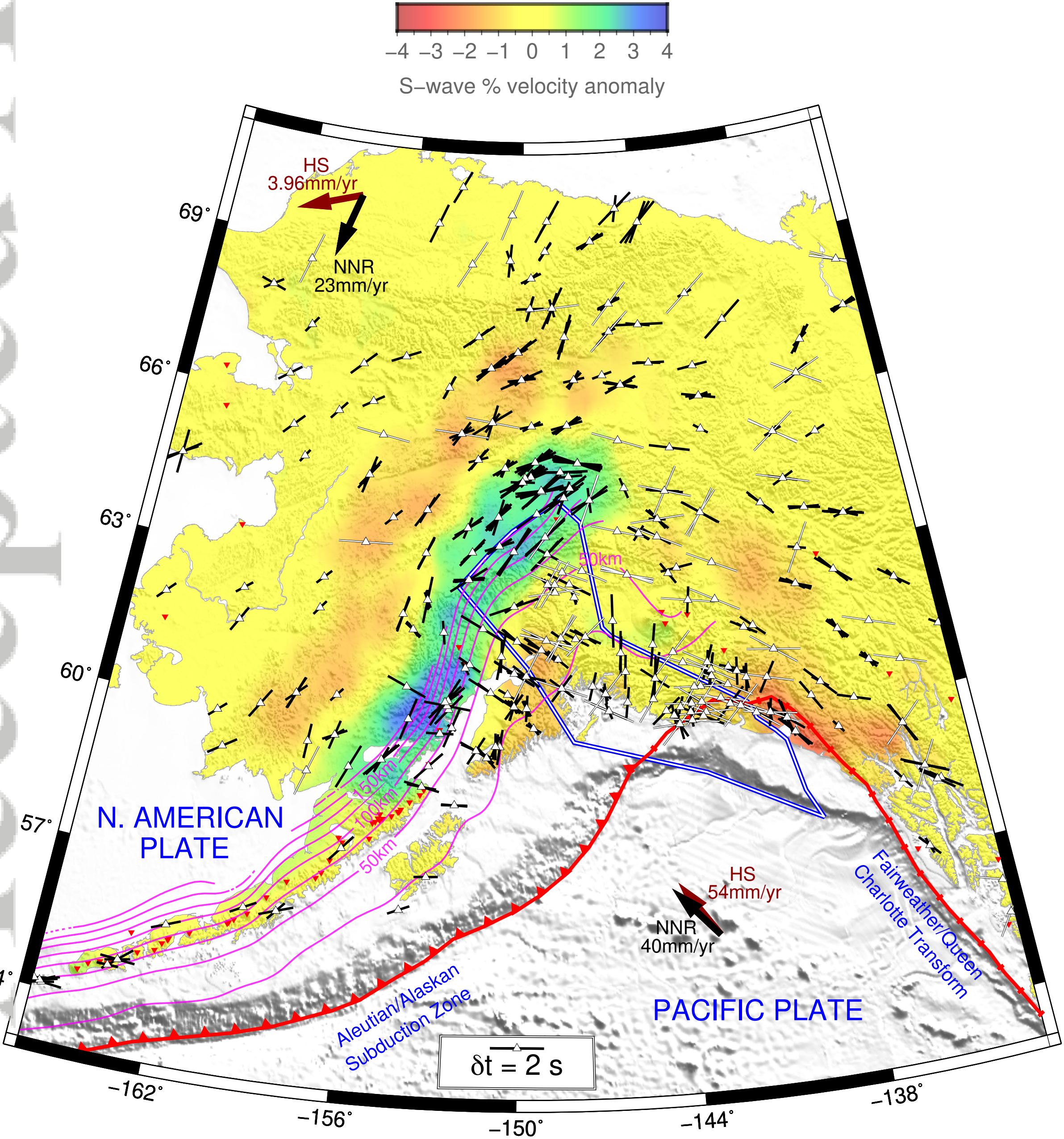

−4 −3 −2 −1 0 1 2 3 4
S−wave % velocity anomaly
HS
3.96mm/yr
NNR
23mm/yr
69°
66°
63°
60°
57°
54°
50km
150km
100km
50km
N. AMERICAN
PLATE
HS
54mm/yr
NNR
40mm/yr
Fairweather/Queen
Charlotte Transform
PACIFIC PLATE
Aleutian/Alaskan
Subduction Zone
δt = 2 s
−162°
−156°
−150°
−144°
−138°

Figure7.

Accepted Article

©2018 American Geophysical Union. All rights reserved.

Accepted Article

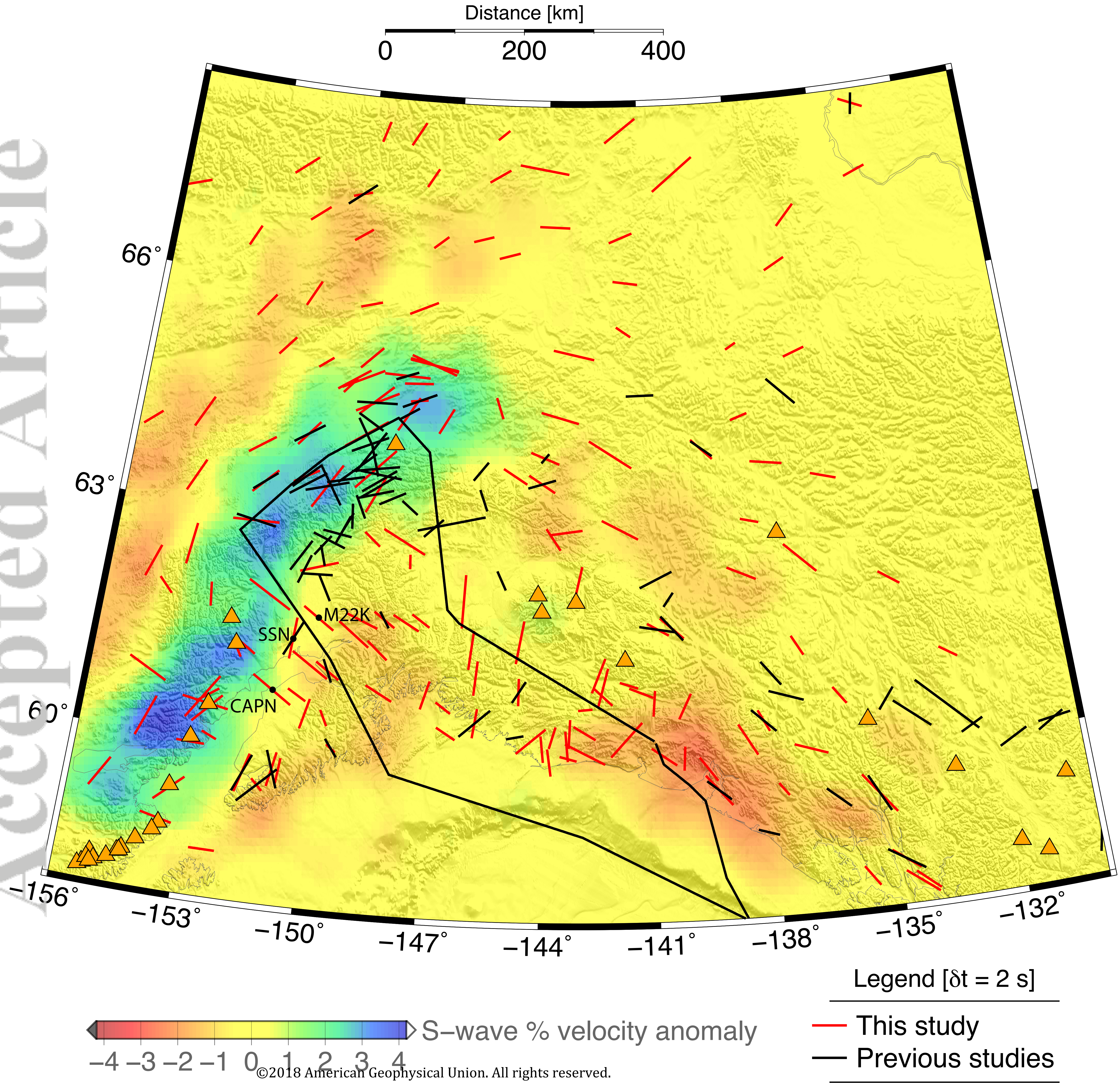

©2018 American Geophysical Union. All rights reserved.

Figure8.

Accepted Article

©2018 American Geophysical Union. All rights reserved.

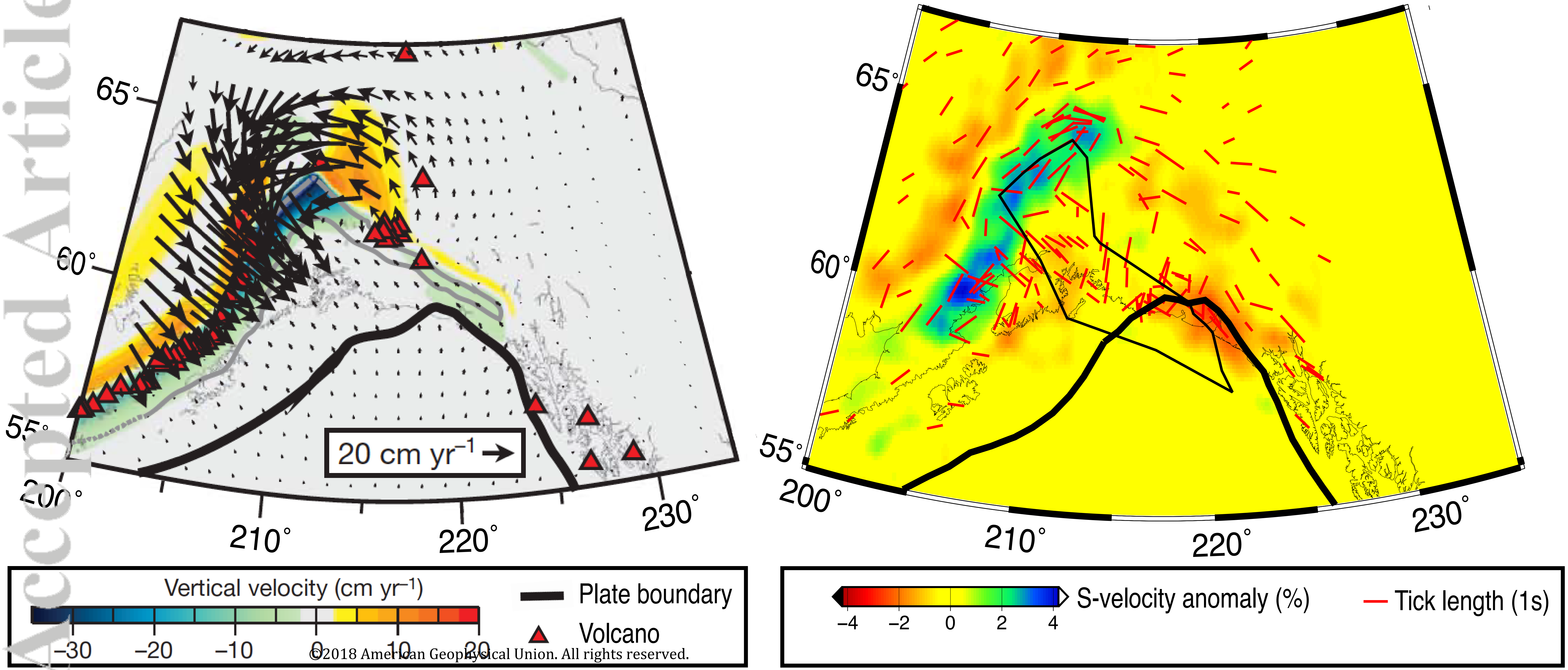

Accepted Article

©2018 American Geophysical Union. All rights reserved.

Figure9.

Accepted Article

©2018 American Geophysical Union. All rights reserved.

Accepted Article

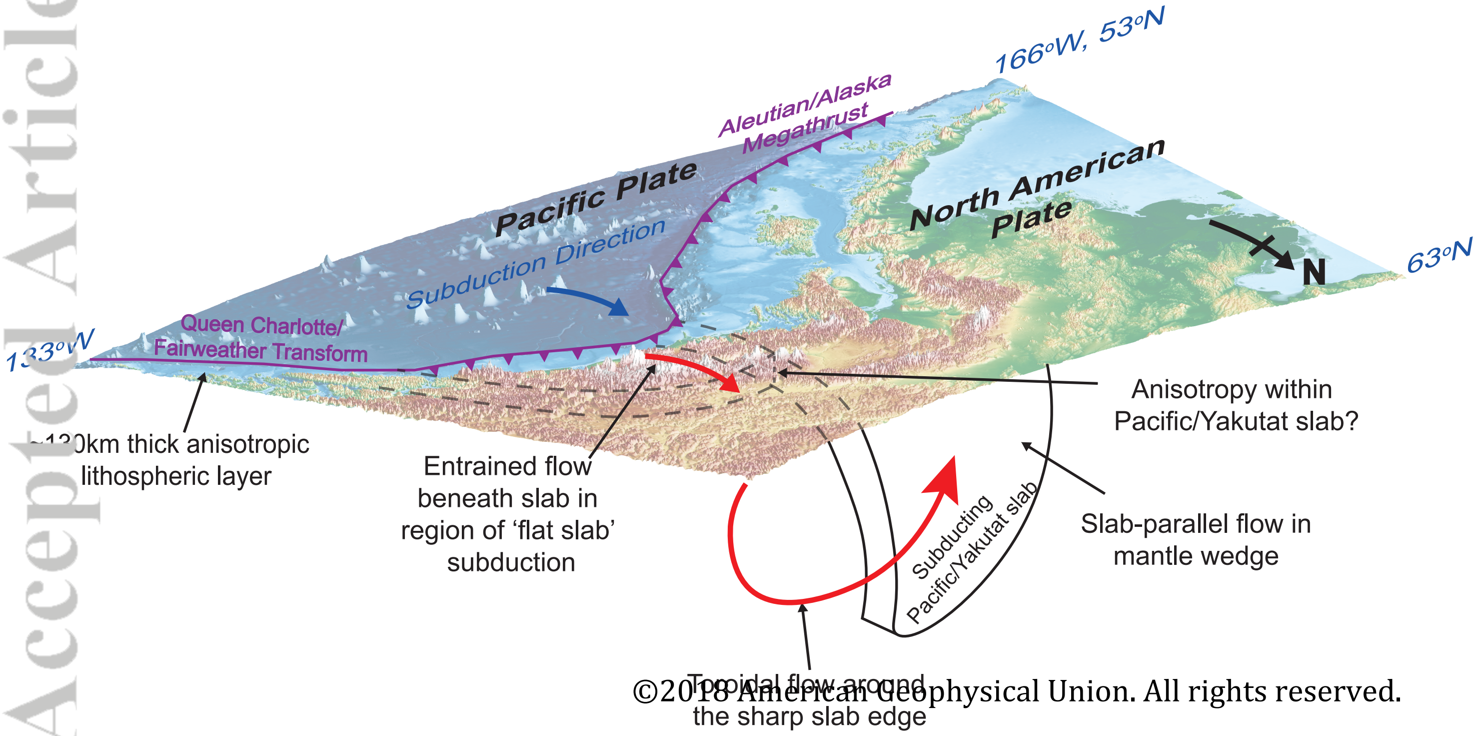

©2018 American Geophysical Union. All rights reserved.